Article

Neuron

Brain Somatic Mutations in *MTOR* Disrupt Neuronal Ciliogenesis, Leading to Focal Cortical Dyslamination

Highlights

- Brain somatic mutations in *MTOR* result in defective neuronal ciliogenesis
- The aberrant accumulation of OFD1 by impaired autophagy disrupts neuronal ciliogenesis
- Defective ciliogenesis accounts for cortical dyslamination in FMCDs
- Defective ciliogenesis abrogates Wnt signaling essential for neuronal polarization

Authors

Sang Min Park, Jae Seok Lim, Suresh Ramakrishina, ..., Dong Seok Kim, Hyongbum (Henry) Kim, Jeong Ho Lee

Correspondence

jhlee4246@kaist.ac.kr

In Brief

Park et al. demonstrate that brain somatic mutations in *MTOR* result in defective neuronal ciliogenesis in FMCDs. The aberrant accumulation of OFD1 by impaired autophagy is responsible for defective ciliogenesis. Moreover, defective ciliogenesis accounts for cortical dyslamination in FMCDs by compromising Wnt signals.

Park et al., 2018, Neuron *99*, 83–97
July 11, 2018
https://doi.org/10.1016/j.neuron.2018.05.039

CellPress

Neuron
Article

Brain Somatic Mutations in *MTOR* Disrupt Neuronal Ciliogenesis, Leading to Focal Cortical Dyslamination

Sang Min Park,[1] Jae Seok Lim,[2] Suresh Ramakrishina,[3] Se Hoon Kim,[4] Woo Kyeong Kim,[2] Junehawk Lee,[5] Hoon-Chul Kang,[6] Jeremy F. Reiter,[7] Dong Seok Kim,[8] Hyongbum (Henry) Kim,[9] and Jeong Ho Lee[1,2,10,11,*]
[1]Biomedical Science and Engineering Interdisciplinary Program, Korea Advanced Institute of Science and Technology (KAIST), Daejeon 34141, Republic of Korea
[2]Graduate School of Medical Science and Engineering, Korea Advanced Institute of Science and Technology (KAIST), Daejeon 34141, Republic of Korea
[3]Graduate School of Biomedical Science and Engineering, Hanyang University, Seoul 04763, Republic of Korea
[4]Department of Pathology, Yonsei University College of Medicine, Seoul 03722, Republic of Korea
[5]Biomedical HPC Technology Research Center, KISTI, Daejeon 34141, Republic of Korea
[6]Division of Pediatric Neurology, Department of Pediatrics, Pediatric Epilepsy Clinics, Severance Children's Hospital, Epilepsy Research Institute, Yonsei University College of Medicine, Seoul 03722, Republic of Korea
[7]Department of Biochemistry and Biophysics, Cardiovascular Research Institute, University of California, San Francisco, San Francisco, CA 94158, USA
[8]Pediatric Neurosurgery, Severance Children's Hospital, Department of Neurosurgery, Yonsei University College of Medicine, Seoul 03722, Republic of Korea
[9]Department of Pharmacology, Brain Korea 21 Plus Project for Medical Sciences, Severance Biomedical Science Institute, Yonsei University College of Medicine, Seoul 03722, Republic of Korea
[10]Center for Synaptic Brain Dysfunctions, Institute for Basic Science, Daejeon 34141, Republic of Korea
[11]Lead Contact
*Correspondence: jhlee4246@kaist.ac.kr
https://doi.org/10.1016/j.neuron.2018.05.039

SUMMARY

Focal malformations of cortical development (FMCDs), including focal cortical dysplasia (FCD) and hemimegalencephaly (HME), are major etiologies of pediatric intractable epilepsies exhibiting cortical dyslamination. Brain somatic mutations in *MTOR* have recently been identified as a major genetic cause of FMCDs. However, the molecular mechanism by which these mutations lead to cortical dyslamination remains poorly understood. Here, using patient tissue, genome-edited cells, and mouse models with brain somatic mutations in *MTOR*, we discovered that disruption of neuronal ciliogenesis by the mutations underlies cortical dyslamination in FMCDs. We found that abnormal accumulation of OFD1 at centriolar satellites due to perturbed autophagy was responsible for the defective neuronal ciliogenesis. Additionally, we found that disrupted neuronal ciliogenesis accounted for cortical dyslamination in FMCDs by compromising Wnt signals essential for neuronal polarization. Altogether, this study describes a molecular mechanism by which brain somatic mutations in *MTOR* contribute to the pathogenesis of cortical dyslamination in FMCDs.

INTRODUCTION

Focal malformations of cortical development (FMCDs), including hemimegalencephaly (HME) and focal cortical dysplasia (FCD), are a heterogeneous group of cortical abnormalities that are highly associated with medically intractable epilepsy, intellectual disability, developmental delay, and autism-spectrum disorders (Foldvary-Schaefer et al., 2004; Lim and Crino, 2013; Wegiel et al., 2010). Despite a broad spectrum of cortical abnormalities in FMCDs, defective neuronal migration and cortical dyslamination are considered common pathological hallmarks (Foldvary-Schaefer et al., 2004). The genetic etiologies of FCD and HME, however, have only recently begun to be uncovered. We and other study groups have found that brain somatic mutations in *MTOR* (mechanistic target of rapamycin) cause both FCD and HME, suggesting that a common molecular mechanism related to the mTOR pathway underlies cortical abnormalities (Crino, 2016; D'Gama et al., 2015, 2017; Lee et al., 2012a; Lim et al., 2015; Mirzaa et al., 2016; Møller et al., 2016; Nakashima et al., 2015). MTOR is a highly conserved serine/threonine kinase and a well-studied central regulator of the mTOR pathway, the activation of which inhibits autophagy process (Laplante and Sabatini, 2012). Nonetheless, the molecular mechanisms by which brain somatic mutations in *MTOR* lead to cortical dyslamination and malpositioned neurons in FMCDs remain unclear.

A precisely regulated process, neuronal migration in the cerebral cortex is important to the formation of neuronal circuitry (Ayala et al., 2007; Evsyukova et al., 2013). Proper, coordinated intracellular responses to extracellular guidance cues are

essential for the migration of neurons from their zone of origin to their destination in the cortex, and neuronal misplacement resulting from defects therein leads to abnormal cortical function (Ayala et al., 2007; Evsyukova et al., 2013; Gleeson and Walsh, 2000). Among organelles in the cell that sense extracellular cues, primary cilia, which are non-motile, microtubule-based organelles, are known to integrate many important signaling pathways, such as Wnt, Sonic hedgehog (Shh), and platelet-derived growth factor (PDGF) (Bangs and Anderson, 2016; Corbit et al., 2005; Hilgendorf et al., 2016; May-Simera and Kelley, 2012), thereby regulating vertebrate development and homeostasis (Goetz and Anderson, 2010; Guemez-Gamboa et al., 2014). In the brain, neuronal cilia are implicated in cortical patterning, neurogenesis, neuronal maturation, and cerebellar development (Lee and Gleeson, 2010). In a recent report, primary cilia were found to play a guiding role in the migration and placement of developing interneurons mediating Shh signaling (Baudoin et al., 2012; Higginbotham et al., 2012, 2013). Neuronal cilia-mediated signaling has been shown to be essential for the initial formation of radial progenitor scaffolds and, when disrupted, to cause aberrant neuronal placement (Higginbotham et al., 2013). Also, genes linked to ciliopathies, a group of syndromic disorders caused by ciliary dysfunction, affect the cortical development including neural progenitor development, neuronal radial migration, neuronal differentiation, and early neuronal connectivity (Guo et al., 2015). However, the role of primary cilia in the pathogenesis of FMCDs, especially defects of radially migrating neurons, caused by brain somatic mutations in *MTOR* is unclear.

In the present study, we observed severely defective neuronal ciliogenesis not only in brain tissues from FMCD patients, but also in a CRISPR-Cas9 genome-edited cell line and mouse models with brain somatic mutation in *MTOR*. We then discovered that brain somatic mutations in *MTOR* elicited severely defective neuronal ciliogenesis by disturbing the autophagy process. Abnormal accumulation of OFD1 protein at centriolar satellites due to disturbed autophagy resulted in defective neuronal ciliogenesis. We further noted that defective neuronal ciliogenesis caused cortical dyslamination in FMCDs by disturbing Wnt signaling. Taken together, our results highlight a molecular mechanism by which brain somatic mutations in *MTOR* contribute to the pathogenesis of cortical dyslamination in FMCDs.

RESULTS

Brain Somatic Mutations in *MTOR* Result in Defective Neuronal Ciliogenesis

HME and FCD patients exhibit cortical dyslamination with dysmorphic neurons and catastrophic epilepsy that is medically intractable, and surgical resection of the affected brain is necessary to alleviate epileptic episodes (Figure 1A). To examine whether neuronal cilia are defective in FMCD patients with brain somatic mutations in *MTOR*, we immunostained for the ciliary marker Arl13b in surgically resected brain tissues from HME and FCD patients with brain somatic mutations in *MTOR* (Table S1). We found that neuronal ciliogenesis was severely disrupted and that ciliary length was significantly decreased in FMCD brain tissue with cytomegalic neurons, compared to non-FMCD brain tissue (Figures 1B–1D). Also, defective neuronal ciliogenesis was observed in brain tissues from tuberous sclerosis complex (TSC) patients, which is another subtype of FMCD caused by a germline mutation in *TSC2* leading to the hyperactivation of MTOR kinase (Figures S1A–S1D; Table S1). These results suggest that defective neuronal ciliogenesis is highly associated with FMCDs.

Next, to investigate whether brain somatic mutations in *MTOR* are causative for defective neuronal ciliogenesis, we generated *in vitro* and *in vivo* models of brain somatic mutations in *MTOR*. Brain somatic mutations in MTOR residue p.Cys1483 have been recurrently found in FMCD patients, including those with FCD and HME (D'Gama et al., 2015; Lee et al., 2012a; Lim et al., 2015). An MTOR p.Cys1483Arg somatic mutation has also been found in FCD patients and characterized *in vitro* as an mTOR kinase-activating mutation (Lim et al., 2015). Two independent studies have reported an MTOR p.Cys1483Tyr mutation in HME, which also appears to be an activating mutation (D'Gama et al., 2015; Lee et al., 2012a). We also found an HME patient with an MTOR p.Cys1483Tyr somatic mutation in our cohort using deep targeted sequencing, followed by biological validation of whether malpositioned cytomegalic neurons can carry the MTOR p.Cys1483Tyr somatic mutation (Figures 1A and S2A–S2E; Table S1). However, this mutation has not been fully characterized *in vitro* and *in vivo*. Thus, to explore whether the MTOR p.Cys1483Tyr mutation causes hyperactivation of mTOR kinase, we first transiently transfected MTOR wild-type or mutant plasmids into human embryonic kidney 293T cells (HEK293T). We then performed western blot analysis and found that the MTOR p.Cys1483Tyr mutation induced a robust increase in P-S6 protein without affecting the expression level of MTOR protein itself, compared to MTOR wild-type (Figure S2F). We also pulled down FLAG-tagged MTOR wild-type and p.Cys1483Tyr protein from HEK293T cells expressing each MTOR construct and performed MTOR kinase assay *in vitro*. We found that MTOR p.Cys1483Tyr robustly increased kinase activity (Figure S2G). Furthermore, to test whether somatic mutation of endogenous MTOR protein induces hyperactivation of the mTOR pathway, we modeled *MTOR* c.4448G > A using homology-directed repair (HDR)-mediated genome editing with the CRISPR-Cas9 system. We generated a genome-edited NIH/3T3 cell line carrying the monoallelic *Mtor* c.4448G > A mutation (Figures S2H–S2K; Table S2). We found that phosphorylation of S6 was significantly increased in mutant cells (Figure S2L). Taken together, these results indicated that the brain somatic mutation MTOR p.Cys1483Tyr induces hyperactivation of mTOR kinase.

Next, we examined whether expression of the MTOR p.Cys1483Tyr somatic mutation in the developing cortex is sufficient to cause cortical dyslamination, spontaneous behavioral seizures, and cytomegalic neurons, which are commonly observed in FMCD patients, including HME, FCD, and TSC (Foldvary-Schaefer et al., 2004; Lim and Crino, 2013). To model a somatic activating mutation in MTOR during cortical development, we performed in utero electroporation to introduce pCIG-MTOR wild-type or p.Cys1483Tyr-IRES-EGFP plasmids into the focal cortical area at embryonic day 14 (E14), when the labeled neurons located to cortical layers II–IV (Tabata and Nakajima,

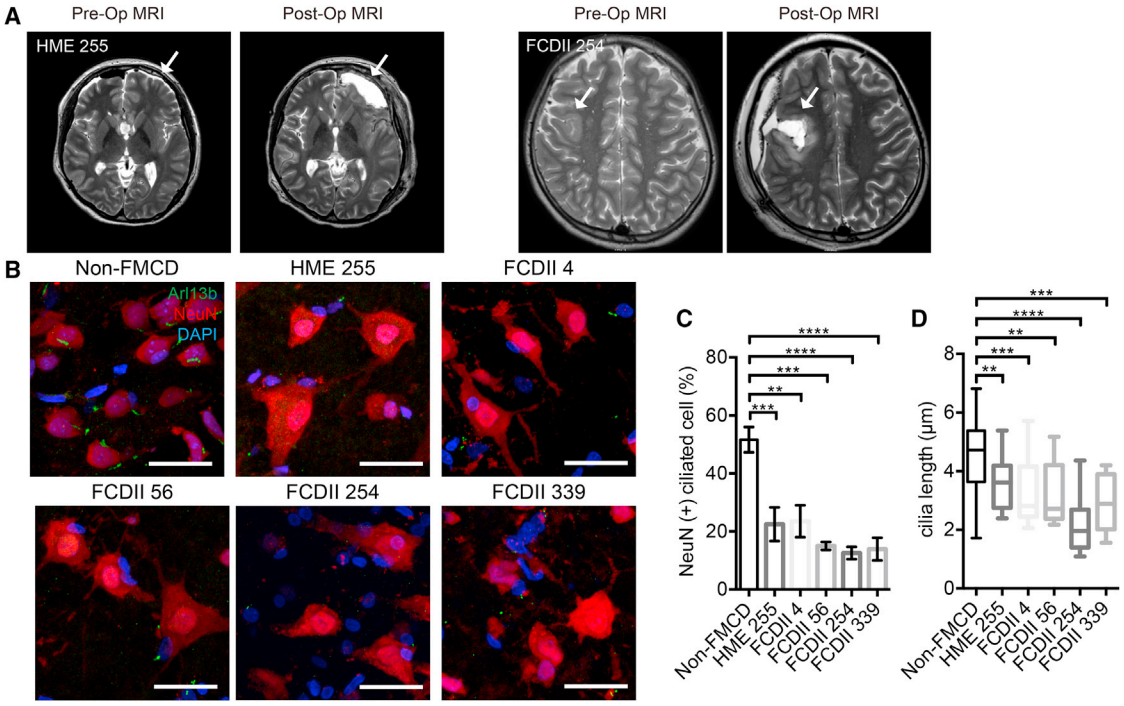

Figure 1. Brain Somatic Mutations in *MTOR* Result in Defective Neuronal Ciliogenesis in FMCD Patients

(A) Representative brain MRIs of patients with FMCDs including HME and FCD type II (FCD II). Arrows indicate the surgically resected brain region in FMCD patients. Pre-Op, pre-operation; Post-Op, post-operation.

(B) Immunostaining for Arl13b and NeuN with DAPI co-staining in brain tissue from FMCD patients. Scale bars, 30 μm.

(C) Bar graph shows the percentage of NeuN-positive ciliated cells (n = 3 experiments; $^{**}p < 0.01$, $^{***}p < 0.001$, and $^{****}p < 0.0001$; one-way ANOVA with Bonferroni's multiple comparison tests).

(D) Bar graph shows the length of primary cilia (non-FMCD, n = 32 cilia; HME 255, n = 19 cilia; FCDII 4, n = 17 cilia; FCDII 56, n = 9 cilia; FCDII 254, n = 14 cilia; FCDII 339, n = 10 cilia; $^{**}p < 0.01$, $^{***}p < 0.001$, and $^{****}p < 0.0001$; one-way ANOVA with Bonferroni's multiple comparison tests).

All data are presented as mean ± SEM. See also Figures S1 and S2 and Table S1.

2001). We performed immunostaining and western blot analysis for P-S6 and MTOR protein in mouse brain tissues electroporated with MTOR wild-type and p.Cys1483Tyr constructs (Figures S3A–S3C). We observed a significant increase in P-S6 protein in MTOR p.Cys1483Tyr-expressing mice brain tissue, compared to MTOR wild-type-expressing mice brain tissue (Figures S3A–S3C). Also, we found no significant difference in the expression levels of MTOR protein between MTOR wild-type- and p.Cys1483Tyr-expressing neurons (Figure S3A). We then measured the distribution of radially migrating neurons and cortical lamination at E18, 4 days after electroporation. Compared with MTOR wild-type-expressing mice, MTOR p.Cys1483Tyr-expressing mice showed disruption of cortical layers II–IV upon staining for Cux1 (cut-like homeobox 1), as well as aberrant distribution of GFP-positive neurons throughout the cortex (Figures 2A–2C). However, there were no significant differences in the intensity of other layer markers, such as Ctip2 (COUP-TF-interacting protein 2) (a marker for layer V) and Tbr1 (T-box, brain 1) (a marker for layer VI) (Figures S3D, S3E, S3G, and S3H). Also, there were no significant changes in the identities of electroporated neurons corresponding to Cux1, Ctip2, and Tbr1 (Figures 2D, S3F, and S3I). Next, we sought to determine whether focal cortical expression of MTOR p.Cys1483Tyr is sufficient to induce spontaneous behavioral seizures and cytomegalic neurons. Following in utero electroporation at E14, we selected GFP-expressing pups at birth (postnatal day 0, P0). After weaning, we monitored these mice for seizures using video recordings (12 hr/day) and electroencephalography (EEG) recordings (6 hr/day). Thirteen of the 14 (93.3%) mice expressing MTOR p.Cys1483Tyr showed spontaneous seizures and epileptic discharges, including high-voltage fast activities (Figures 2E and 2F). In contrast, control mice expressing MTOR wild-type showed no behavioral or electrographic seizures (Figures 2E and 2F). Furthermore, we measured the soma size of MTOR p.Cys1483Tyr-expressing neurons, compared with that of MTOR wild-type-expressing neurons, and found that soma size was increased in MTOR p.Cys1483Tyr-expressing neurons (Figures 2G and 2H). After the mice (>P56) were injected daily via an intraperitoneal route with 10 mg/kg of rapamycin, an mTOR inhibitor, for 2 weeks, the increased soma size was significantly rescued (Figures 2G and 2H). These data indicated that our mouse model of the somatic activating mutation MTOR p.Cys1483Tyr can recapitulate clinical and pathological phenotypes common among FMCD patients, including cortical dyslamination, seizures, and cytomegalic neurons.

To determine whether somatic activating mutations in *MTOR* affect the formation of primary cilia, we performed

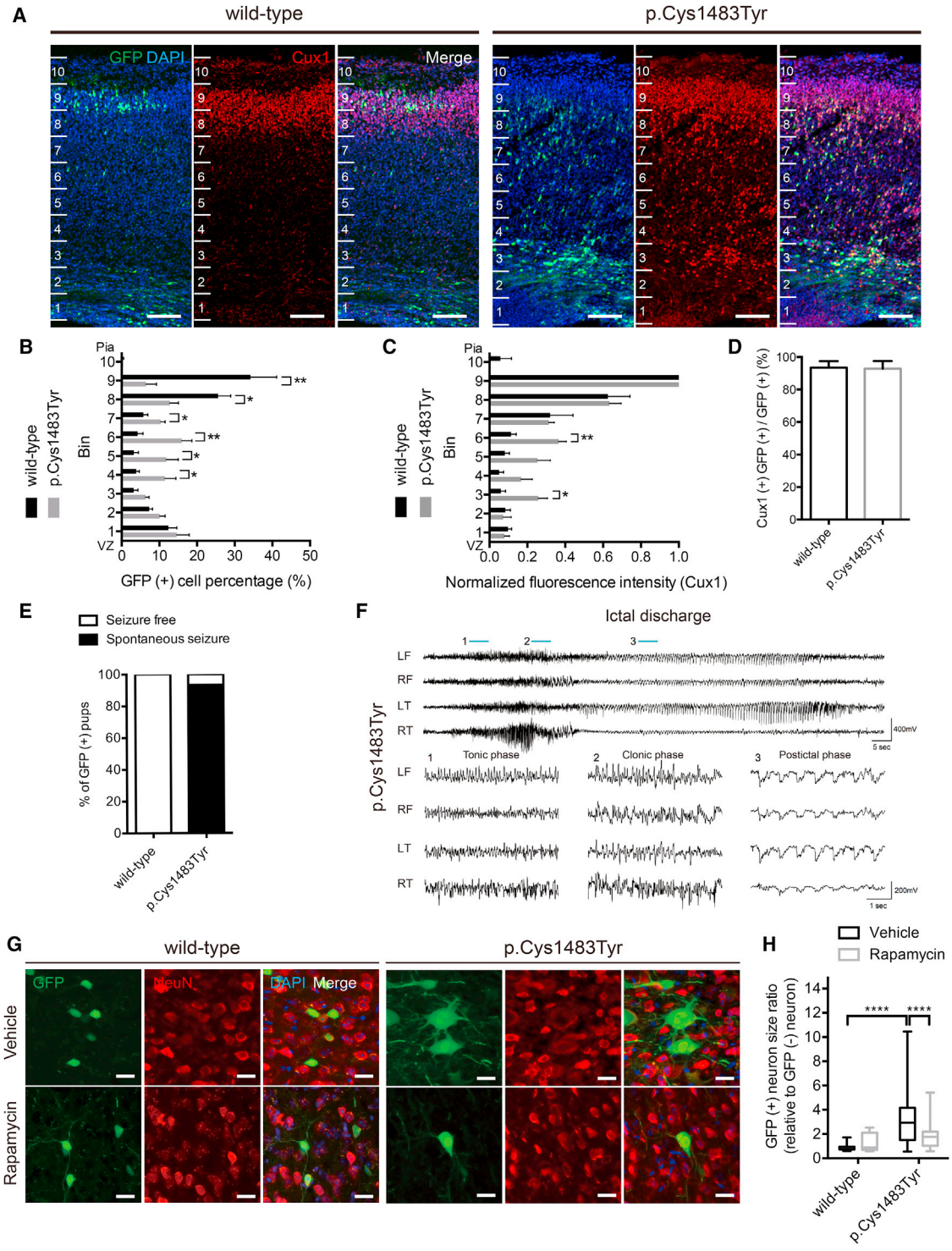

Figure 2. Mouse Model of the Brain Somatic Mutation MTOR p.Cys1483Tyr Recapitulates Clinical and Pathological Phenotypes Found in FMCD Patients

(A) Immunostaining for Cux1 with DAPI co-staining in coronal sections of embryonic mouse brains (E18). Scale bars, 100 μm.

(B) Bar graph shows the percentage of GFP-positive cells reflecting the distribution of electroporated cells within the developing mouse neocortex (wild-type, n = 5 mice; p.Cys1483Tyr, n = 6 mice; *p < 0.05 and **p < 0.01; Student's t test).

(C) Bar graph shows the normalized fluorescence intensities for Cux1 (wild-type, n = 5 mice; p.Cys1483Tyr, n = 6 mice; *p < 0.05 and **p < 0.01; Student's t test).

(legend continued on next page)

immunostaining for primary cilia in MTOR p.Cys1483Tyr genome-edited NIH/3T3 cells, as well as cells transiently transfected with MTOR p.Cys1483Tyr plasmid after serum-starved conditions for 24 hr. MTOR mutant cells showed a robust decrease in ciliary length and number of ciliated cells, as labeled with any one of several ciliary markers, including Arl13b (ADP-ribosylation factor-like protein 13B), Ac-tub (acetylated tubulin), and GT335 (polyglutamylated tubulin) (Figures S4A–S4C). Treatment with the mTOR inhibitors torin-1 (200 nM) and rapamycin (200 nM) during serum-starved conditions for 24 hr restored ciliogenesis (Figures 3A–3C). Consistent with these data, wild-type NIH/3T3 cells transiently transfected with the MTOR mutant plasmid also showed defective ciliogenesis rescued by rapamycin treatment (Figures S4D–S4F). We then examined whether MTOR p.Cys1483Tyr somatic mutation disturbs neuronal ciliogenesis *in vivo*. To do so, we performed immunostaining for the neuronal cilia marker ACIII (adenylyl cyclase type 3) in brain slices from MTOR p.Cys1483Tyr-expressing mice (>P56) presenting cortical dyslamination, seizures, and cytomegalic neurons. Compared with MTOR wild-type-expressing neurons, we found that the formation of neuronal primary cilia was markedly reduced in MTOR p.Cys1483Tyr-expressing neurons (Figures 3D and 3E). Similar to the *in vitro* results, intraperitoneal injection of rapamycin (10 mg/kg/day) for 2 weeks rescued the defective neuronal ciliogenesis in MTOR p.Cys1483Tyr-expressing neurons (Figures 3D and 3E).

We recently reported on another somatic activating mutation in *MTOR*, MTOR p.Leu2427Pro, that was found in patients with FCD and caused FMCD-related phenotypes *in vivo* (Lim et al., 2015). To test whether this somatic mutation also disrupts ciliogenesis, we transfected the pCIG-MTOR p.Leu2427Pro-IRES-EGFP plasmid into wild-type NIH/3T3 cells and performed immunostaining for Ac-tub and Arl13b under serum-starved conditions. In line with results obtained with MTOR p.Cys1483Tyr-expressing cells, we observed defective ciliogenesis in MTOR p.Leu2427Pro-expressing cells, which was rescued by treatment with rapamycin (200 nM) under serum-starved conditions (Figures S4D–S4F). Moreover, we performed in utero electroporation of a pCIG-MTOR p.Leu2427Pro-IRES-EGFP plasmid into the developing mouse cortex and observed a significant decrease in the number of ciliated neurons in MTOR p.Leu2427Pro-expressing mice (>P56). Also, treatment with rapamycin (10 mg/kg per day) for 2 weeks rescued the defective neuronal ciliogenesis caused by MTOR p.Leu2427Pro-expression (Figures S4G and S4H). Taken together, these results suggest that brain somatic activating mutations in *MTOR*, which are causative for FMCDs, disrupt the formation of neuronal primary cilia.

Brain Somatic Mutation in *MTOR* Leads to Impaired Autophagy and Aberrant Accumulation of OFD1 Centriolar Satellite Protein

The mTOR kinase is a negative regulator of autophagy (Laplante and Sabatini, 2012). Interestingly, a recent study reported that autophagy promotes ciliogenesis at the cellular level by removing the autophagy substrate OFD1 from centriolar satellites (Tang et al., 2013). OFD1 is a key regulator of ciliogenesis at centrioles, and inherited mutations in the *OFD1* gene cause ciliopathies, such as oral-facial-digital syndrome and Joubert syndrome (Coene et al., 2009; Ferrante et al., 2001; Singla et al., 2010b). Thus, we hypothesized that inhibition of autophagy caused by the *MTOR* somatic mutation would cause an aberrant accumulation of OFD1 at centriolar satellites, thereby potentially disrupting neuronal ciliogenesis. To test our hypothesis, we performed western blot analysis to examine whether MTOR mutant cells show an increase in OFD1 or inhibition of autophagy as marked by decreases in LC3-II and increases in p62 protein. Compared with wild-type NIH/3T3 cells, serum-starved MTOR mutant cells showed increased OFD1 protein, decreased LC3-II, and increased p62 levels, reflective of autophagy inhibition (Figure S5A). The mTOR inhibitors torin-1 (200 nM) and rapamycin (200 nM) rescued the aberrant increases in OFD1, as well as the autophagy deficiency, in MTOR mutant cells (Figure S5A). Next, we performed immunostaining for p62 and OFD1. Consistent with results of western blot analyses, we observed significant increases in the number of p62 puncta in the cytoplasm of MTOR mutant cells, as well as MTOR p.Cys1483Tyr-expressing neurons of our mouse model (>P56) (Figures 4A–4D). We also observed an increase in p62 puncta in neurons expressing another MTOR somatic activating mutation, p.Leu2427Pro (Figures S5B and S5C). In addition, treatment with 40 μM chloroquine (CQ), an autophagy inhibitor, under serum-starved conditions significantly decreased the number of primary cilia in wild-type NIH/3T3 cells, while there was no significant change in ciliogenesis in MTOR mutant cells (Figures S5D–S5F). Further, although OFD1 was only located at centrioles labeled with acetylated and γ-tubulin in wild-type cells under serum-starved conditions, we noted aberrant accumulation of OFD1 at centriolar

(D) Bar graph shows the percentage of Cux1-positive electroporated cells (wild-type, n = 5 mice; p.Cys1483Tyr, n = 6 mice; *p < 0.05 and **p < 0.01; Student's t test).

(E) Spontaneous seizures were observed in mice expressing MTOR p.Cys1483Tyr and wild-type, based on the video-EEG recordings (wild-type, n = 8 mice; p.Cys1483Tyr, n = 15 mice).

(F) EEG recording of ictal discharges from an MTOR p.Cys1483Tyr-carrying mouse. The ictal discharges with convulsive seizure are divided into three phases (tonic, clonic, and postictal). A detailed analysis of each phase corresponding to the blue bar is shown with an expanded scale. The EEG pattern of tonic and clonic phases (blue bars #1 and #2) shows low-amplitude, high-frequency polyspikes and a relatively high-amplitude, rhythmic pattern, respectively. The EEG pattern in the postictal phase (blue bar #3) represents the synchronized attenuation of amplitude. LF, left frontal lobe; RF, right frontal lobe; LT, left temporal lobe; RT, right temporal lobe.

(G) Immunostaining for NeuN with DAPI co-staining in a section of the mice cortex (>P56). The soma size of GFP-positive neurons was measured. Scale bars, 20 μm.

(H) Bar graph shows neuron size in each group in affected cortical regions (wild-type with vehicle, n = 35 cells; wild-type with rapamycin, n = 5 cells; p.Cys1483Tyr with vehicle, n = 168 cells; p.Cys1483Tyr with rapamycin, n = 173 cells; ****p < 0.0001; Student's t test).

All data are presented as mean ± SEM. See also Figure S3.

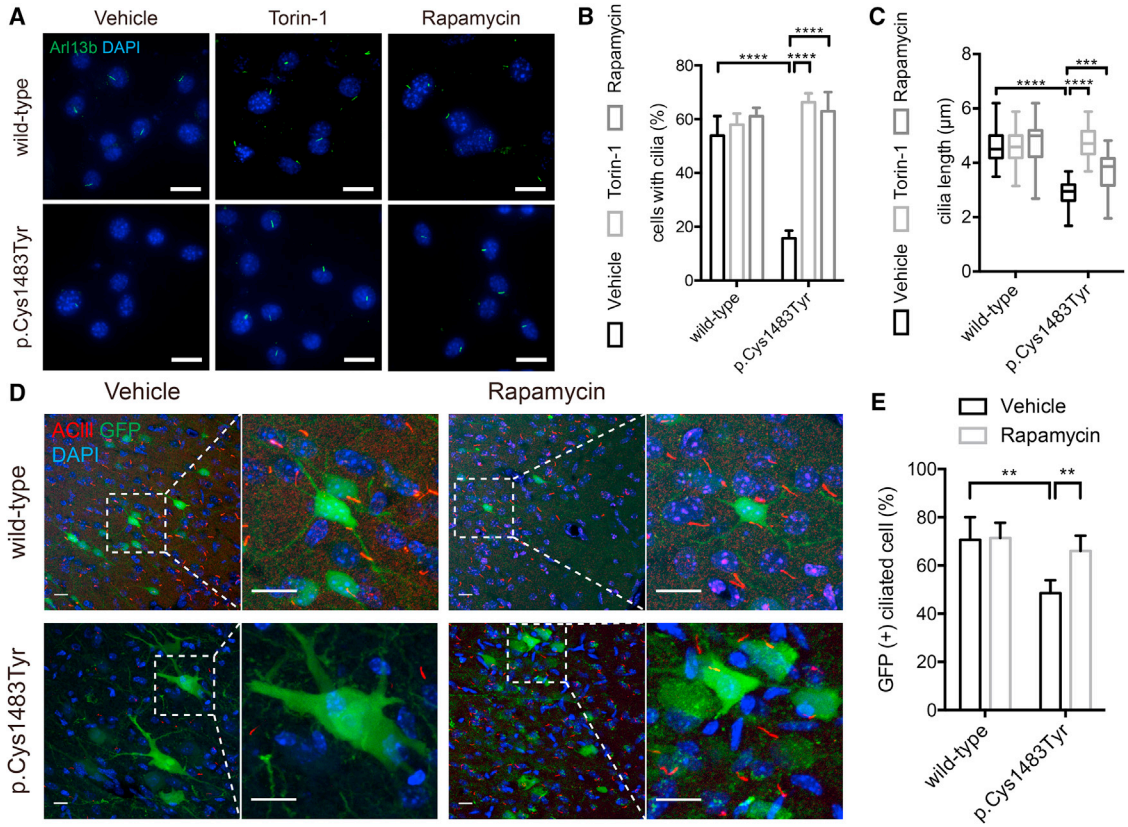

Figure 3. The Brain Somatic Mutation MTOR p.Cys1483Tyr Disrupts Ciliogenesis *In Vitro* and *In Vivo*

(A) Immunostaining for Arl13b with DAPI co-staining in MTOR wild-type and mutant NIH/3T3 cell lines. Scale bars, 20 μm.

(B) Bar graph shows the percentage of ciliated cells (n = 4 experiments; ****p < 0.0001; one-way ANOVA with Bonferroni's multiple comparison tests).

(C) Bar graph shows the lengths of primary cilia (wild-type with vehicle, n = 37 cilia; wild-type with torin-1, n = 43 cilia; wild-type with rapamycin, n = 29 cilia; p.Cys1483Tyr with vehicle, n = 16 cilia; p.Cys1483Tyr with torin-1, n = 42 cilia; p.Cys1483Tyr with rapamycin, n = 67 cilia; **p < 0.01 and ****p < 0.0001; one-way ANOVA with Bonferroni's multiple comparison tests).

(D) Immunostaining for ACIII with DAPI co-staining in affected cortical regions of MTOR wild-type- or p.Cys1483Tyr-expressing mice (>P56). Scale bars, 15 μm.

(E) Bar graph shows the percentage of GFP-positive ciliated cells (wild-type with vehicle, n = 4 mice; wild-type with rapamycin, n = 4 mice; p.Cys1483Tyr with vehicle, n = 5 mice; p.Cys1483Tyr with rapamycin, n = 5 mice; **p < 0.01; one-way ANOVA with Bonferroni's multiple comparison tests).

All data are presented as mean ± SEM. See also Figure S4.

satellites around the centriole in MTOR mutant NIH/3T3 cells (Figures 4E–4G). These data suggest that the *MTOR* somatic mutations found in FMCD patients cause the inhibition of autophagy and aberrant accumulation of OFD1 at centriolar satellites, implying that failure of autophagy-mediated degradation of OFD1 may be responsible for defective neuronal ciliogenesis.

In addition to autophagy, MTOR can regulate the cell cycle and actin cytoskeletal rearrangement (Fingar et al., 2004; Jacinto et al., 2004; Sarbassov et al., 2004), which can impact the formation of primary cilia: for example, entry into the cell cycle induces the disassembly of primary cilia (Nigg and Stearns, 2011). To examine whether the MTOR p.Cys1483Tyr somatic mutation disrupts ciliogenesis by dysregulating the cell cycle, we performed immunostaining for Ki67, an indicator of cell proliferation. We found that there was no significant difference in the percentage of Ki67-positive cells between wild-type and MTOR mutant NIH/3T3 cells under untreated and serum-starved conditions (Figures S5G and S5H). Then, we examined the cell cycle of MTOR p.Cys1483Tyr-carrying neurons *in vivo* at E16 by performing Ki67, PH3 (phospho-histone H3), and BrdU (bromodeoxyuridine) staining. We injected BrdU (100 mg/kg) intraperitoneally 2 hr before brain preparation. As a result, we found that the percentage of electroporated neurons positive for each marker was not significantly changed in MTOR p.Cys1483Tyr-expressing mice, compared to MTOR wild-type-expressing mice (Figures S5I–S5N). Meanwhile, stabilization of the actin cytoskeleton negatively regulates ciliogenesis, whereas cytochalasin D, an inhibitor of actin polymerization, promotes ciliogenesis by destabilizing the actin cytoskeleton (Cao et al., 2012; Kim et al., 2010, 2015; Sharma et al., 2011). We found that treatment with cytochalasin D (100 nM) did not induce ciliogenesis in MTOR mutant cells, compared with wild-type NIH/3T3 cells (Figures S5O and S5P). These results suggest that cell-cycle abnormalities and actin stabilization are not associated with the disruption of ciliogenesis caused by MTOR p.Cys1483Tyr somatic mutation.

Next, we examined whether the autophagy process is inhibited and whether OFD1 protein levels are aberrantly increased in FMCD brain tissues. We performed immunostaining

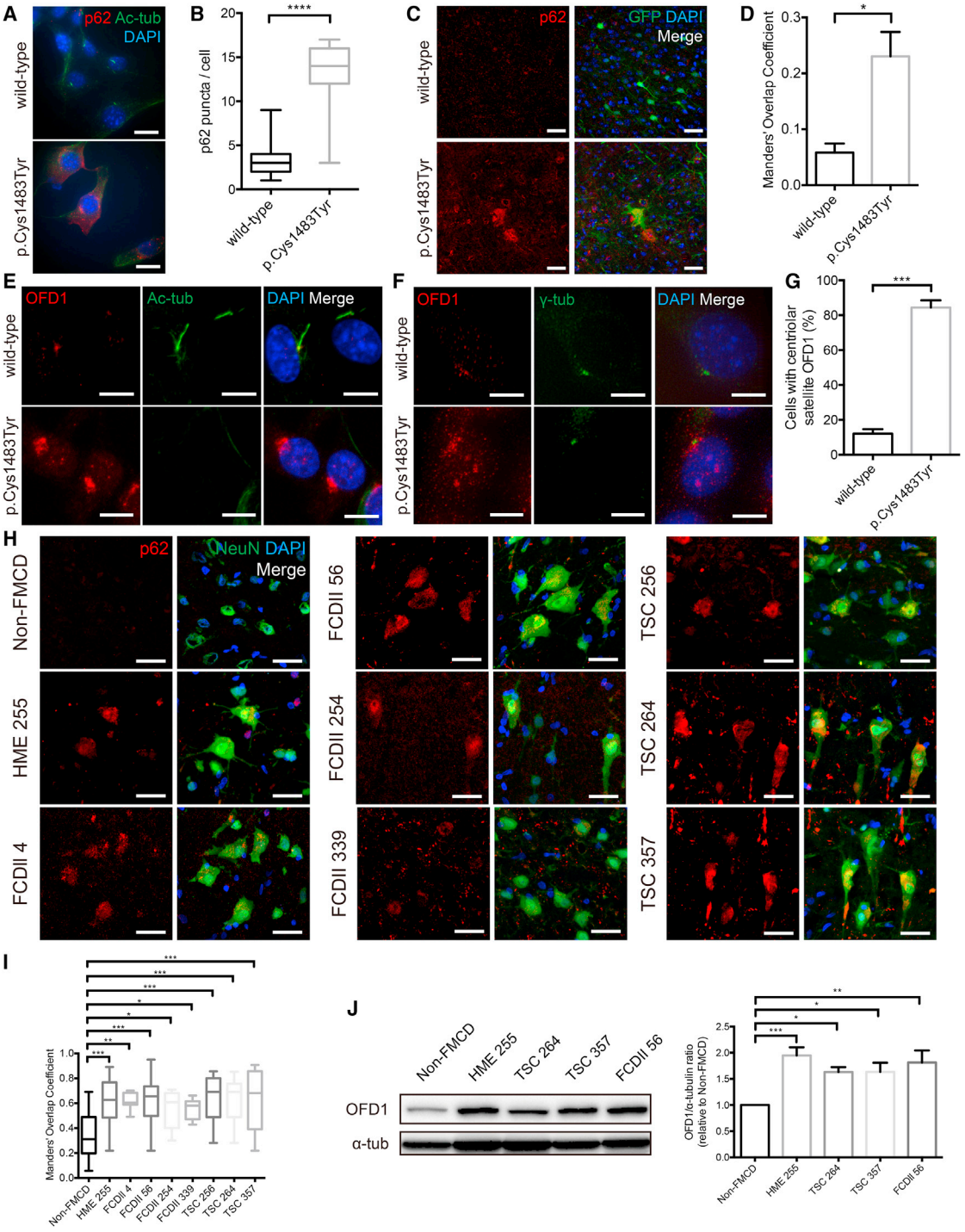

Figure 4. Brain Somatic Mutation in *MTOR* Leads to Impaired Autophagy and Aberrant Accumulation of OFD1 Centriolar Satellite Protein

(A) Immunostaining for p62 and Ac-tub with DAPI co-staining in MTOR wild-type and mutant NIH/3T3 cell lines. Scale bars, 20 μm.

(B) Bar graph shows the number of p62 puncta per cell (wild-type, n = 42 cells; p.Cys1483Tyr, n = 56 cells; ***p < 0.001; Student's t test).

(C) Immunostaining for p62 with DAPI co-staining in cortical regions of adult mice (>P56) shows an increase in p62 levels in MTOR p.Cys1483Tyr-expressing neurons. Scale bars, 30 μm.

(D) Bar graph showing the Manders' overlap coefficient (wild-type, n = 4 mice; p.Cys1483Tyr, n = 4 mice; *p < 0.05; Student's t test).

(E) Immunostaining for OFD1 and Ac-tub with DAPI co-staining in MTOR wild-type and mutant NIH/3T3 cell lines. Scale bars, 10 μm.

(F) Immunostaining for OFD1 and γ -tubulin with DAPI co-staining in MTOR wild-type and mutant NIH/3T3 cell lines. Scale bars, 10 μm.

(G) Bar graph shows the percentage of cells with centriolar satellite OFD1 (n = 3 experiments; ***p < 0.001; Student's t test).

(legend continued on next page)

of p62 and observed marked increases in p62 puncta in cytomegalic neurons in brain tissue from HME and FCD patients (Figures 4H and 4I). Inhibited autophagy was also observed by immunostaining of p62 in brain tissue from TSC patients (Figures 4H and 4I). Consistent with our findings, a recent report indicated that defective autophagy is associated with dysmorphic neurons in FCD and TSC brain specimens (Yasin et al., 2013). In western blot analysis of OFD1, we found significantly greater accumulation of the OFD1 protein in brain tissue from FMCD patients with HME, FCD, and TSC, compared to non-FMCD brain tissue (Figure 4J). These results suggest that brain somatic mutation in *MTOR* leads to impaired autophagy and aberrant accumulation of OFD1 centriolar satellite protein.

The Aberrant Accumulation of OFD1 Caused by Impaired Autophagy Is Responsible for Defective Neuronal Ciliogenesis

To test the possibility of whether autophagy-mediated degradation of OFD1 is required for neuronal ciliogenesis, we sought to determine whether knockdown of *Ofd1* would restore ciliogenesis in MTOR p.Cys1483Tyr mutant cells. After selecting the most efficient short hairpin RNA (shRNA) sequence against *Ofd1* (*Ofd1* shRNA #3) (Figure S6A), we transfected the *Ofd1* shRNA plasmid containing a GFP reporter into MTOR mutant NIH/3T3 cells and found that the accumulation of OFD1 at centriolar satellites disappeared under serum-starved conditions (Figures S6B and S6C). Furthermore, we found that the knockdown of *Ofd1* was able to restore ciliogenesis in MTOR mutant cells (Figures 5A and 5B). Importantly, to verify whether knockdown of *Ofd1* restores neuronal ciliogenesis *in vivo*, we performed in utero electroporation of the p.Cys1483Tyr mutant plasmid with *Ofd1* shRNA. Consistent with the *in vitro* results, knockdown of *Ofd1* rescued defective neuronal ciliogenesis in MTOR p.Cys1483Tyr-expressing neurons (>P56) (Figures 5C, 5D, and S6D). These data indicate that *MTOR* somatic mutation induces aberrant accumulation of OFD1 and that the accumulation of OFD1 is responsible for defective neuronal ciliogenesis.

Next, we examined whether the impaired autophagy caused by *MTOR* somatic mutation accounts for OFD1 accumulation and defective neuronal ciliogenesis. The autophagy-related protein ATG5 is essential for formation of the autophagosome, and ATG5 deficiency impairs autophagy (Mizushima et al., 1998, 2001; Suzuki et al., 2001). ATG5 is also critical for early brain development, in which it is involved in cortical neurogenesis and astrocyte differentiation (Lv et al., 2014; Wang et al., 2014). A recent study showed that ATG5 deficiency disrupts ciliogenesis in murine fibroblasts and kidney cells (Tang et al., 2013). Thus, to test whether autophagy mediates neuronal ciliogenesis by degrading OFD1 *in vivo*, we performed in utero electroporation of an *Atg5* shRNA plasmid containing a GFP reporter at E14 and found that it was able to reduce the expression level of Atg5 protein in the developing cortex (E16), as measured by immunostaining and western blot analysis of brain lysates (Figures 5E, S6E, and S6F). Also, we observed increased p62 puncta in the cytoplasm of *Atg5* shRNA-expressing neurons (>P21) (Figures S6G and S6H). Furthermore, we found significant perturbation of neuronal ciliogenesis in *Atg5* shRNA-expressing neurons (>P56) (Figures 5F and 5G) and increased OFD1 protein levels in lysates of affected cortical areas (Figure 5E). Collectively, these results suggest that the *MTOR* somatic mutations found in FMCD patients induce aberrant accumulation of OFD1 by impairing autophagy, thereby eliciting defective neuronal ciliogenesis.

Disruption of Autophagy-Mediated Neuronal Ciliogenesis Leads to Cortical Dyslamination in FMCDs by Disturbing Wnt Signaling

We further examined whether the disruption of neuronal ciliogenesis contributes to pathological phenotypes of FMCDs, such as cortical dyslamination, cytomegalic neurons, and epilepsy, which were successfully phenocopied in MTOR p.Cys1483Tyr-expressing mice. To do this, we examined which phenotype could be alleviated by the restoration of neuronal ciliogenesis upon *Ofd1* knockdown in MTOR p.Cys1483Tyr-expressing mice. Surprisingly, *Ofd1* knockdown in MTOR p.Cys1483Tyr-expressing mice (E18) considerably restored defective neuronal migration and cortical dyslamination, compared to MTOR p.Cys1483Tyr-expressing mice (Figures S6I–S6K). This restoration of neuronal migration and cortical dyslamination was also observed in adult mouse brains expressing MTOR p.Cys1483Tyr with *Ofd1* shRNA, especially in cortical layer V to layers II–IV (Figures 6A and 6B). However, *Ofd1* knockdown did not affect spontaneous behavioral seizures or cytomegalic neurons present in the MTOR p.Cys1483Tyr-expressing mice (Figures S6L–S6P). These results indicate that defective neuronal ciliogenesis elicited by somatic activating mutation in *MTOR* underlies cortical dyslamination, but not behavioral seizures and dysmorphic neurons.

Additionally, the results implied that autophagy-mediated neuronal ciliogenesis, compromised by *MTOR* somatic mutation, promotes proper cortical lamination. To test this, we further examined whether the disruption of autophagy-mediated neuronal ciliogenesis is responsible for the abnormal neuronal migration and cortical dyslamination observed in FMCDs. We knocked down *Atg5* in developing cortical neurons *in vivo* and found that knockdown of *Atg5* resulted in a decrease in the number of GFP-positive neurons in the upper cortical plate and a robust increase in the number of GFP-positive neurons in the lower cortical plate, suggestive of defective migration (Figures 6C and 6D). In addition, we performed immunostaining for Cux1 (a marker for the cortical layer II–IV)

(H) Immunostaining for p62 and NeuN with DAPI co-staining in brain tissue of FMCD patients, including HME, FCD, and TSC. Scale bars, 30 μm.
(I) Bar graph shows the Manders' overlap coefficient (non-FMCD, n = 15 cells; HME 255, n = 18 cells; FCDII 4, n = 12 cells; FCDII 56, n = 24 cells; FCDII 254, n = 11 cells; FCDII 339, n = 12 cells; TSC 256, n = 13 cells; TSC 264, n = 21 cells; TSC 357, n = 23 cells; $^{*}p < 0.05$, $^{**}p < 0.01$, and $^{***}p < 0.001$ compared with non-FMCD; one-way ANOVA with Bonferroni's multiple comparison tests).
(J) Western blot analysis for OFD1 in lysates from patient brain tissues. Band intensities were quantified (n = 4 experiments; $^{*}p < 0.05$, $^{**}p < 0.01$, and $^{***}p < 0.001$; one-way ANOVA with Bonferroni's multiple comparison tests).
All data are presented as mean ± SEM. See also Figure S5.

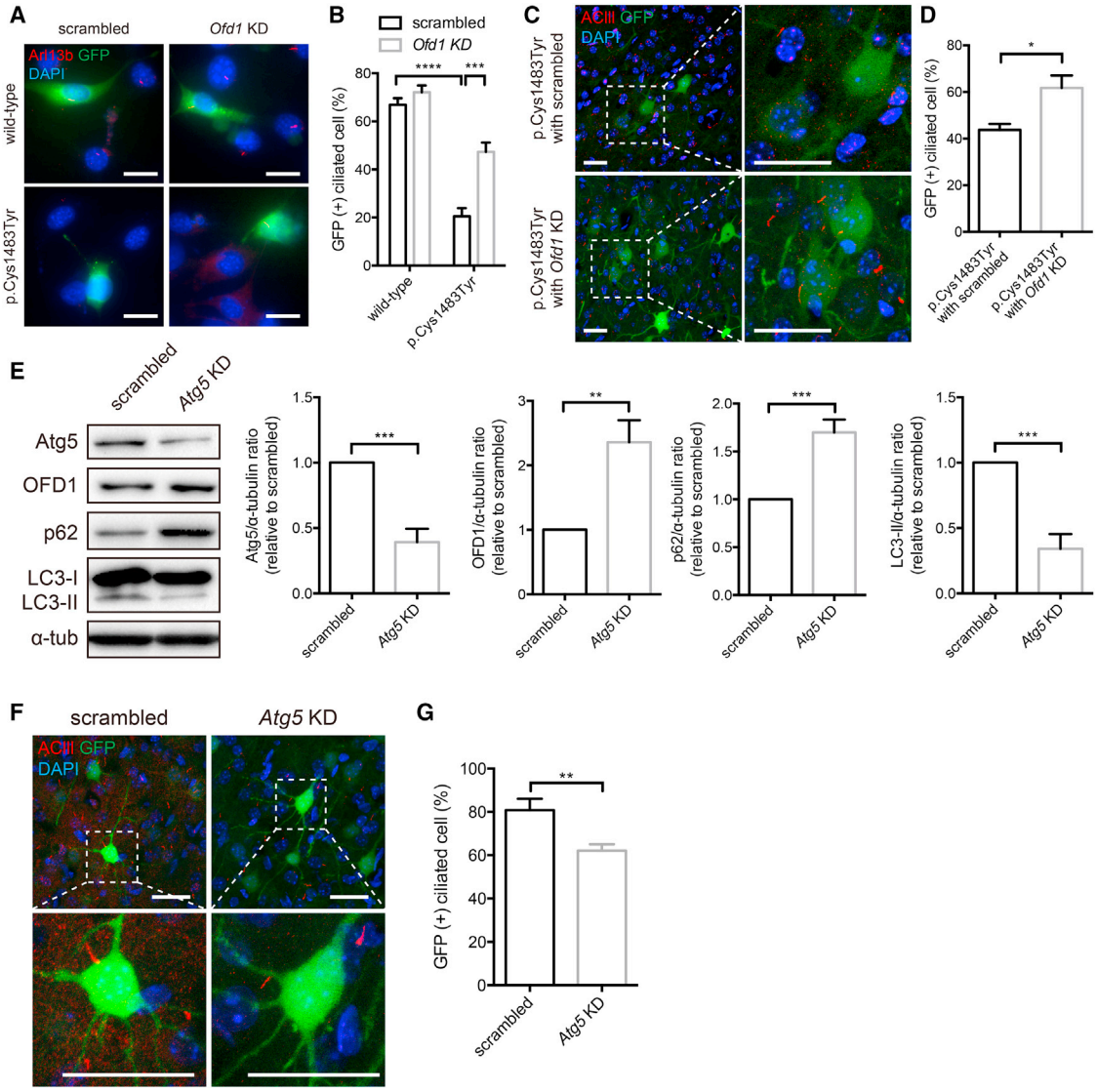

Figure 5. The Aberrant Accumulation of OFD1 Caused by Impaired Autophagy Is Responsible for Defective Neuronal Ciliogenesis

(A) Immunostaining for Arl13b with DAPI co-staining in MTOR wild-type and mutant NIH/3T3 cell lines, with or without knockdown of *Ofd1*. Scale bars, 20 μm.

(B) Bar graph shows the percentage of GFP-positive ciliated cells (n = 5 experiments; ***p < 0.001 and ****p < 0.0001; one-way ANOVA with Bonferroni's multiple comparison tests).

(C) Immunostaining for ACIII with DAPI co-staining in cortical regions of adult mice (>P56) shows the recovery of neuronal ciliogenesis through knockdown of *Ofd1* in MTOR p.Cys1483Tyr-expressing neuron. Scale bars, 30 μm.

(D) Bar graph shows the percentage of GFP-positive ciliated cells (p.Cys1483Tyr with scrambled, n = 5 mice; p.Cys1483Tyr with *Ofd1* knockdown, n = 7 mice; *p < 0.05; Student's t test).

(E) Western blot analysis of lysates from scrambled shRNA or *Atg5* shRNA electroporated cortical regions at E16. Band intensities were measured (n = 5 experiments; *p < 0.05 and **p < 0.01; Student's t test).

(F) Immunostaining for ACIII with DAPI co-staining in affected cortical regions of scrambled and *Atg5* knocked-down (*Atg5* knockdown) adult mice (>P56). Scale bars, 30 μm.

(G) Bar graph shows the percentage of GFP-positive ciliated cells in affected cortical regions (scrambled, n = 4 mice; *Atg5* knockdown, n = 6 mice; **p < 0.01; Student's t test).

All data are presented as mean ± SEM. See also Figure S6.

and found that cortical lamination was disrupted in mice upon knockdown of *Atg5* (Figures 6C and 6E). As expected, knockdown of *Atg5* did not result in either seizures or cytomegalic neurons (Figures S6Q–S6S). Thus, these data suggest that autophagy-mediated neuronal ciliogenesis by degradation of OFD1 is critical for proper neuronal migration and cortical lamination and, when disrupted by *MTOR* somatic mutation, causes cortical dyslamination in FMCDs.

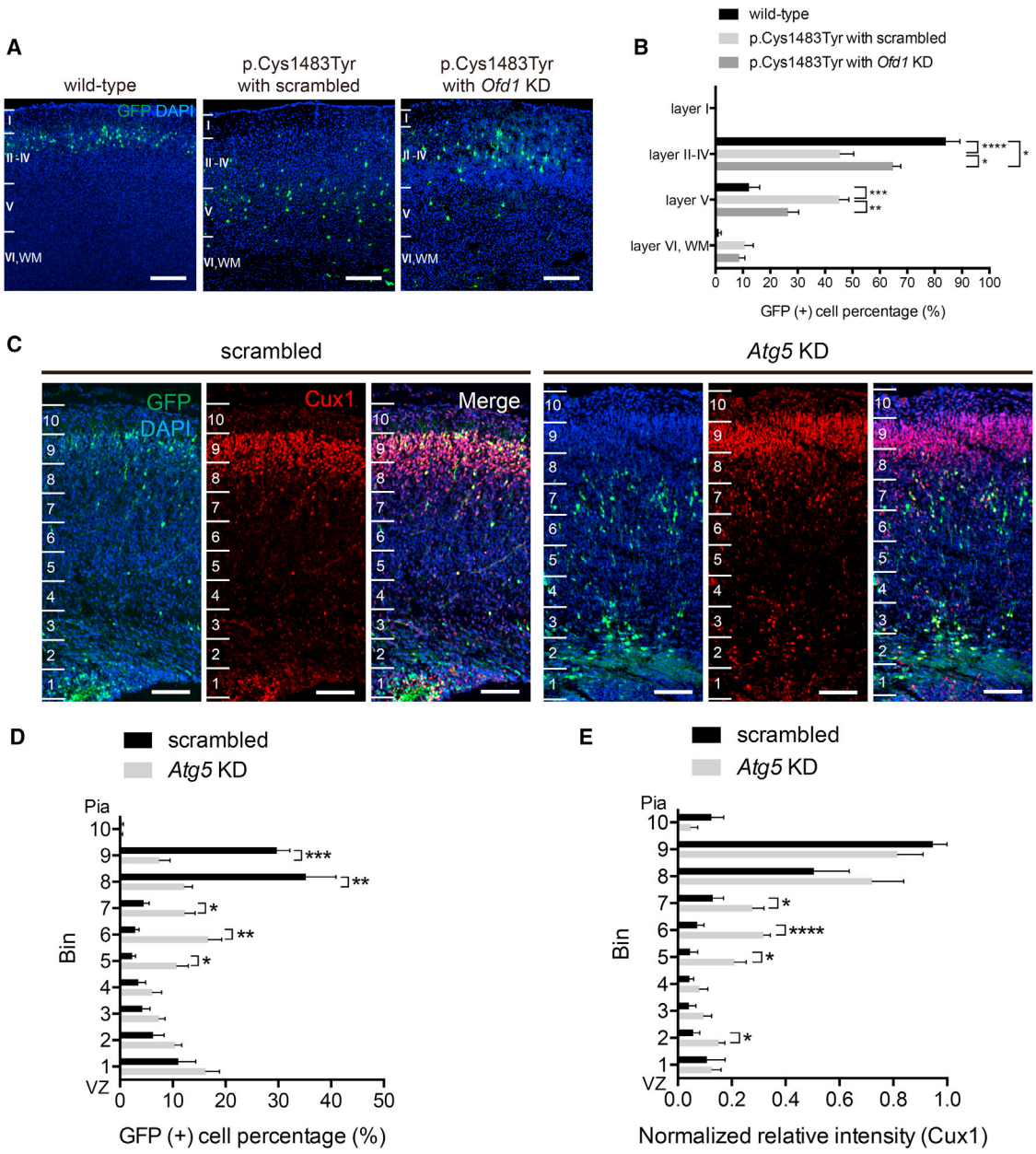

Figure 6. Disruption of Autophagy-Mediated Neuronal Ciliogenesis Leads to Cortical Dyslamination in FMCD

(A) Immunostaining showing the position of GFP-positive neurons in cortical layers from MTOR wild-type- and p.Cys1483Tyr-expressing adult mice (>P56) with scrambled or *Ofd1* shRNA. Scale bars, 200 μm.

(B) Distribution of GFP-positive neurons in each cortical layer (wild-type, n = 4 mice; p.Cys1483Tyr with scrambled, n = 6 mice; p.Cys1483Tyr with *Ofd1* knockdown, n = 7 mice; *p < 0.05, **p < 0.01, ***p < 0.001, and ****p < 0.0001; one-way ANOVA with Bonferroni's multiple comparison tests).

(C) Immunostaining for Cux1 with DAPI co-staining in cortical regions at E18. Scale bars, 100 μm.

(D) Bar graph showing the percentage of GFP-positive cells reflecting the distribution of electroporated cells within the developing mouse neocortex at E18 (scrambled, n = 4 mice; *Atg5* knockdown, n = 6 mice; *p < 0.05, **p < 0.01, and ***p < 0.001; Student's t test).

(E) Bar graph shows the normalized fluorescence intensities for Cux1 (scrambled, n = 4 mice; *Atg5* knockdown, n = 6 mice; *p < 0.05 and ****p < 0.0001; Student's t test).

All data are presented as means ± SEM. See also Figure S6.

Next, we investigated the mechanism by which impaired neuronal ciliogenesis causes disrupted migration of cortical neurons. Primary cilia integrate various signaling pathways, including Wnt, Shh, PDGF, and GPCR signaling (Bangs and Anderson, 2016; Corbit et al., 2005; Hilgendorf et al., 2016; May-Simera and Kelley, 2012). Among these signaling

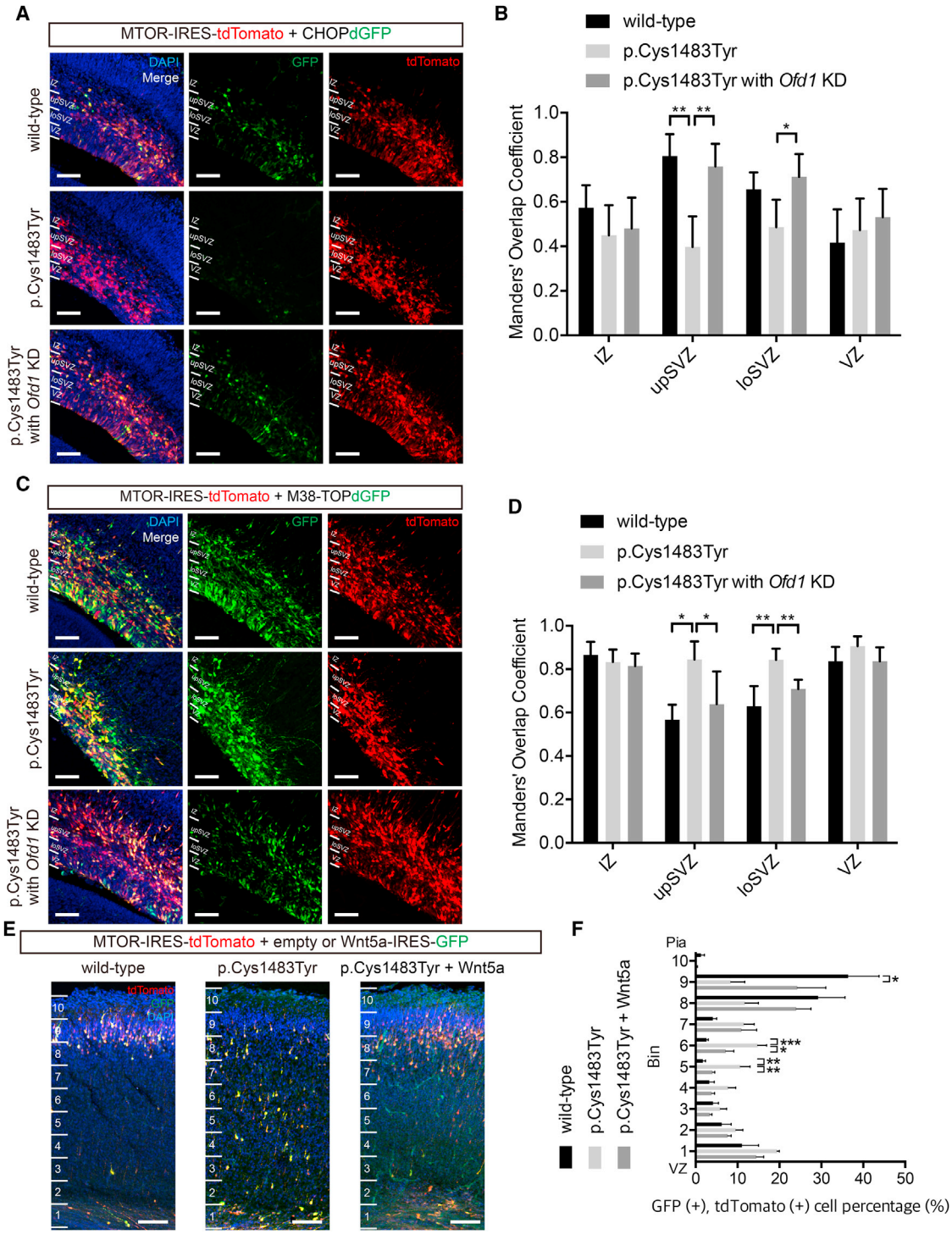

Figure 7. Defective Neuronal Ciliogenesis Abrogates Wnt Signaling in the SVZ, Thereby Disrupting Proper Cortical Lamination

(A) Fluorescence images with DAPI staining in coronal sections of embryonic mouse brains (E16). Scale bars, 75 μm. VZ, ventricular zone; loSVZ, lower subventricular zone; upSVZ, upper subventricular zone; IZ, intermediate zone.

(B) Bar graph shows the Manders' overlap coefficient (wild-type, n = 3 mice; p.Cys1483Tyr, n = 5 mice; p.Cys1483Tyr with *Ofd1* knockdown, n = 4 mice; $^{**}p < 0.01$ and $^{***}p < 0.001$; one-way ANOVA with Bonferroni's multiple comparison tests).

(C) Fluorescence images with DAPI staining in coronal sections of embryonic mouse brains (E16). Scale bars, 75 μm.

(D) Bar graph shows the Manders' overlap coefficient (wild-type, n = 3 mice; p.Cys1483Tyr, n = 4 mice; p.Cys1483Tyr with *Ofd1* knockdown, n = 6 mice; $^{*}p < 0.05$, $^{**}p < 0.01$, and $^{***}p < 0.001$; one-way ANOVA with Bonferroni's multiple comparison tests).

(legend continued on next page)

pathways, the Wnt pathway has been implicated in neuronal radial migration and cerebral cortical development (Boitard et al., 2015; Corbit et al., 2008; Gerdes et al., 2007; Munji et al., 2011): for example, transient downregulation of canonical Wnt/β-catenin signaling by an increase of non-canonical Wnt signaling at the upper subventricular zone (upSVZ) underlies multipolar to bipolar transition of migrating neurons, which is necessary for proper cortical lamination (Boitard et al., 2015). To test whether impaired neuronal ciliogenesis abrogates Wnt signaling, we co-electroporated a canonical (M38-TOPdGFP) or non-canonical (CHOPdGFP) Wnt signaling-dependent reporter with MTOR wild-type or p.Cys1483Tyr-expressing plasmids at E14. As a result, we observed aberrant activation of canonical Wnt signaling, whereas non-canonical Wnt signaling was significantly inactivated at the upSVZ of MTOR p.Cys1483Tyr-expressing mice (E16), compared with MTOR wild-type-expressing mice (Figures 7A–7D). Then, we analyzed the polarity of neurons residing in the intermediate zone (IZ) of the developing mice cortex (E18) by measuring the number of primary processes and branch nodes. We found that, while most wild-type neurons showed bipolar stages in IZ, MTOR p.Cys1483Tyr neurons showed multipolar stages with an increased number of branch processes (Figures S7A–S7C). Next, we tested whether the rescue of neuronal cilia by *Ofd1* knockdown could restore dysregulated Wnt signaling and defective neuronal polarity. We found that MTOR p.Cys1483Tyr-expressing mice with *Ofd1* knockdown showed transient downregulation of the canonical Wnt pathway and upregulation of the non-canonical Wnt pathway in the upSVZ accompanied by the restoration of impaired neuronal polarity, similar to MTOR wild-type-expressing mice (Figures 7A–7D and S7A–S7C). These results suggest that dysregulation of the cilia-mediated Wnt pathway by *MTOR* somatic activating mutation may be critical for neuronal migration and proper cortical development. Thus, we further examined whether the restoration of inactivated non-canonical Wnt pathway signaling is sufficient to rescue defective neuronal migration in MTOR p.Cys1483Tyr-expressing mice. To do so, we co-electroporated a Wnt5a-expressing vector, a ligand for non-canonical Wnt pathway signaling, with MTOR p.Cys1483Tyr-expressing plasmid, and observed the restoration of defective neuronal migration, as marked by an increase in the number of electroporated neurons in the upper cortical plate and a decrease in the number of electroporated neurons in the lower cortical plate (Figures 7E, 7F and S7D–S7J). These results demonstrated that defective neuronal ciliogenesis abrogates Wnt signaling in the SVZ, thereby disrupting proper cortical lamination. Taken together, all of these results suggest that disruption of autophagy-mediated neuronal ciliogenesis leads to cortical dyslamination in FMCDs with brain somatic mutations in *MTOR* by disturbing Wnt signaling.

DISCUSSION

Herein, we outlined the molecular genetic mechanism of how brain somatic mutations in *MTOR* lead to focal cortical dyslamination commonly found in patients with FMCDs. We observed severely defective neuronal ciliogenesis not only in FMCD patients with brain somatic mutation in *MTOR*, but also in a genome-edited cell line and an in utero electroporated mouse model carrying somatic activating mutation in *MTOR*. Next, we observed that inhibition of autophagy by *MTOR* somatic activating mutation induced the aberrant accumulation of OFD1 at centriolar satellites in the brain tissue of FMCD patients, as well as the *in vitro* and *in vivo* models, which resulted in defective neuronal ciliogenesis. Then, selective knockdown of *Ofd1* was able to rescue disrupted neuronal ciliogenesis in the mouse model, and restoration of neuronal ciliogenesis alleviated cortical dyslamination. We further showed that defective neuronal ciliogenesis abrogated non-canonical Wnt signaling in the upSVZ, thereby disrupting cortical lamination.

HME, FCD, and TSC are the most important causes of intractable epilepsy, developmental delay, and autism-spectrum disorder (Casanova et al., 2013; Palmini and Holthausen, 2013; Schwartzkroin and Walsh, 2000). These conditions present with defective cortical lamination as a common pathological feature (Aronica et al., 2012). Although these conditions are caused by genetic variations that lead to hyperactivation of the PI3K-AKT-mTOR pathway, the molecular mechanism underlying the defective cortical lamination remains poorly understood (Crino, 2016; D'Gama et al., 2015, 2017; Lee et al., 2012a; Lim et al., 2015; Mirzaa et al., 2016; Møller et al., 2016; Nakashima et al., 2015). Recently, Baek and colleagues reported that neural progenitors carrying an activating mutation in AKT3 exert a non-cell-autonomous effect on the migration of neighboring neurons through effects on the secretion of Reelin (Baek et al., 2015). How mutations autonomously affect neuronal migration, however, has yet to be clarified. Our study implies that defects in autophagy-mediated neuronal ciliogenesis underlie the cell-autonomous migration of mutation-carrying neurons, which may be followed by non-cell-autonomous effects on the migration of neighboring neurons. Interestingly, we also observed defective ciliogenesis and impaired autophagy of GFP-negative neurons adjacent to GFP-positive neurons with MTOR mutations (Figures 3D and 4C), implying that non-cell-autonomous effect exerted by somatic mutation in *MTOR* might be associated with this phenomenon. Non-cell-autonomous effect of somatic mutations in MTOR would be an interesting subject worthy of future study.

While neuronal misplacement has frequently been found to be associated with seizures in FMCDs, whether cortical dyslamination is necessary for epileptogenesis in FMCDs is not as clear. Our results indicated that cortical dyslamination in FMCD patients with brain somatic mutations activating the mTOR

(E) Immunostaining showing the position of electroporated neurons in developing mouse neocortices (E18). Scale bars, 100 μm.
(F) Bar graph showing the percentage of GFP-positive cells, reflecting the distribution of electroporated cells within the developing mouse neocortex at E18 (wild-type, n = 5 mice; p.Cys1483Tyr, n = 4 mice; p.Cys1483Tyr + Wnt5a, n = 5 mice; *$p < 0.05$, **$p < 0.01$, and ***$p < 0.001$; one-way ANOVA with Bonferroni's multiple comparison tests).
All data are presented as mean ± SEM. See also Figure S7.

pathway is not necessary for epileptogenesis and neuronal cytomegaly. Consistent with our findings, Hsieh and colleagues recently demonstrated that spontaneous seizures do not require cortical dyslamination in an experimental model of FCD (Hsieh et al., 2016). Although further studies will be necessary for elucidating how the small fraction of neurons with *MTOR* somatic mutation induce intractable seizures, our findings reflect a molecular mechanism of how brain somatic mutations in *MTOR* cell-autonomously induce the defective neuronal migration commonly found in patients with FMCDs.

Ciliopathy describes a group of human syndromic disorders that are caused by ciliary dysfunction, such as Bardet-Biedl syndrome (BBS), Joubert syndrome (JBTS), and orofaciodigital syndrome (OFD) (Reiter and Leroux, 2017). It is well established that almost all underlying genetic causes for ciliopathies are inherited or *de novo* germline mutations in genes encoding proteins that localize to, or function within, the ciliary compartment, thereby affecting multiple organs (Reiter and Leroux, 2017). However, in this study, we discerned that brain somatic mutations in a small subset of neurons are sufficient to cause severely defective neuronal ciliogenesis and that such somatic mutations result in dysfunction of neuronal cilia responsible for focal cortical dyslamination in FMCDs. Thus, our results imply that ciliopathies could also be caused by somatic mutations, in addition to inherited or *de novo* germline mutations. Consistent with this idea, Saitsu and colleagues recently reported that brain-specific somatic mutations in genes encoding ciliary proteins, such as Gli3 and Ofd1, can cause hypothalamic hamartoma (Saitsu et al., 2016). Also, our study suggests that FMCDs caused by brain somatic mutations in mTOR pathway genes are a sporadic form of ciliopathy presenting focal cortical dyslamination.

Neuronal primary cilia are critical for neuronal migration during brain development (Guemez-Gamboa et al., 2014). It was recently reported that primary cilia play a guiding role in the migration and placement of developing interneurons (Baudoin et al., 2012; Higginbotham et al., 2012, 2013). Also, neuronal cilia-mediated signaling is essential for initial formation of radial progenitor scaffolds and, when disrupted, causes aberrant neuronal placement (Higginbotham et al., 2013). Recently, primary cilia in radial glial cells were reported to be critical for brain ventricle morphogenesis and cortical development by regulating the mTORC1 pathway (Foerster et al., 2017). However, the role for primary cilia in radially migrating pyramidal neurons remains unclear. Emerging studies implicate Wnt signaling, which also can be regulated by primary cilia, in neuronal radial migration and cerebral cortical development by promoting neuronal transition from a multipolar to bipolar phase (Boitard et al., 2015; Corbit et al., 2008; Gerdes et al., 2007; Munji et al., 2011). Moreover, it has been shown that the maintenance of appropriate Wnt/β-catenin signaling tone in cortical radial progenitors is necessary for cerebral cortical development (Nakagawa et al., 2017). Like autophagy-deficient neurodevelopmental disorders, many ciliopathies present with defective neuronal migration (Guemez-Gamboa et al., 2014; Guo et al., 2015). To date, however, whether neuronal autophagy and neuronal cilia work cooperatively for proper neuronal migration remains unexplored. Our study revealed a physiological role for autophagy-mediated neuronal ciliogenesis in neuronal migration and cortical lamination mediated by non-canonical Wnt signaling. Taken together, the results of our study not only shed light on a molecular mechanism underlying cortical dyslamination in patients with FMCDs, but also provide insights into the physiological role of autophagy-mediated neuronal ciliogenesis in the human brain.

STAR★METHODS

Detailed methods are provided in the online version of this paper and include the following:

- KEY RESOURCES TABLE
- CONTACT FOR REAGENT AND RESOURCE SHARING
- EXPERIMENTAL MODEL AND SUBJECT DETAILS
  - Subject ascertainment
  - Animals
  - Cell culture
- METHOD DETAILS
  - Targeted hybrid capture sequencing and bioinformatic analysis
  - Plasmids
  - Mutagenesis and cloning of MTOR mutant construct
  - Cas9 and guide RNA constructs
  - T7E1 assay
  - Preparation of single-stranded oligodeoxynucleotides (ssODN)
  - Generation of knock-in clones
  - Pharmacological studies
  - *In vitro* MTOR kinase assay
  - Laser-capture microdissection with the subsequent Sanger sequencing
  - Western blot analysis
  - In utero electroporation and BrdU injection
  - Video-Electroencephalography (EEG) monitoring
  - *In vivo* rapamycin treatment
  - Immunocytochemistry and image analysis
  - Immunohistochemistry and image analysis
- QUANTIFICATION AND STATISTICAL ANALYSIS

SUPPLEMENTAL INFORMATION

Supplemental Information includes seven figures and two tables and can be found with this article online at https://doi.org/10.1016/j.neuron.2018.05.039.

ACKNOWLEDGMENTS

This work was supported by grants from the Korean Health Technology R&D Project, Ministry of Health & Welfare, Republic of Korea (H15C3143 and H16C0415 to J.H.L.); Suh Kyungbae Foundation (to J.H.L.); Citizens United for Research in Epilepsy (to J.H.L.); the NIH (AR054396 and GM095941 to J.F.R.); and IBS-R002-D1 (to J.H.L.).

AUTHOR CONTRIBUTIONS

S.M.P. and J.H.L. conceived and designed the study. J.S.L. and S.M.P. performed genetic studies. S.H.K. performed pathological studies. J.S.L. and J.L. performed bioinformatics analysis. S.M.P. performed *in vitro* studies. S.M.P. and J.S.L. performed immunostaining and *in vivo* studies. S.R. and H.K. designed and performed *in vitro* CRISPR-Cas9 experiments. S.M.P. and J.S.L. performed video-EEG recording and analysis of seizures. D.S.K.,

H.-C.K., S.H.K., and W.K.K. collected patients' samples and managed patients' information and tissue samples. J.F.R. contributed key reagents and advices. S.M.P. and J.H.L. wrote the manuscript with input from all authors.

DECLARATION OF INTERESTS

The authors declare no competing interests.

Received: December 11, 2017
Revised: April 6, 2018
Accepted: May 25, 2018
Published: June 21, 2018

REFERENCES

Aronica, E., Becker, A.J., and Spreafico, R. (2012). Malformations of cortical development. Brain Pathol. *22*, 380–401.

Ayala, R., Shu, T., and Tsai, L.H. (2007). Trekking across the brain: the journey of neuronal migration. Cell *128*, 29–43.

Baek, S.T., Copeland, B., Yun, E.J., Kwon, S.K., Guemez-Gamboa, A., Schaffer, A.E., Kim, S., Kang, H.C., Song, S., Mathern, G.W., and Gleeson, J.G. (2015). An AKT3-FOXG1-reelin network underlies defective migration in human focal malformations of cortical development. Nat. Med. *21*, 1445–1454.

Bangs, F., and Anderson, K.V. (2016). Primary cilia and mammalian hedgehog signaling. Cold Spring Harb. Perspect. Biol. Published online May 1, 2017. https://doi.org/10.1101/cshperspect.a028175.

Baudoin, J.P., Viou, L., Launay, P.S., Luccardini, C., Espeso Gil, S., Kiyasova, V., Irinopoulou, T., Alvarez, C., Rio, J.P., Boudier, T., et al. (2012). Tangentially migrating neurons assemble a primary cilium that promotes their reorientation to the cortical plate. Neuron *76*, 1108–1122.

Boitard, M., Bocchi, R., Egervari, K., Petrenko, V., Viale, B., Gremaud, S., Zgraggen, E., Salmon, P., and Kiss, J.Z. (2015). Wnt signaling regulates multipolar-to-bipolar transition of migrating neurons in the cerebral cortex. Cell Rep. *10*, 1349–1361.

Cao, J., Shen, Y., Zhu, L., Xu, Y., Zhou, Y., Wu, Z., Li, Y., Yan, X., and Zhu, X. (2012). miR-129-3p controls cilia assembly by regulating CP110 and actin dynamics. Nat. Cell Biol. *14*, 697–706.

Casanova, M.F., El-Baz, A.S., Kamat, S.S., Dombroski, B.A., Khalifa, F., Elnakib, A., Soliman, A., Allison-McNutt, A., and Switala, A.E. (2013). Focal cortical dysplasias in autism spectrum disorders. Acta Neuropathol. Commun. *1*, 67.

Cingolani, P., Platts, A., Wang, L., Coon, M., Nguyen, T., Wang, L., Land, S.J., Lu, X., and Ruden, D.M. (2012). A program for annotating and predicting the effects of single nucleotide polymorphisms, SnpEff: SNPs in the genome of Drosophila melanogaster strain w1118; iso-2; iso-3. Fly (Austin) *6*, 80–92.

Coene, K.L., Roepman, R., Doherty, D., Afroze, B., Kroes, H.Y., Letteboer, S.J., Ngu, L.H., Budny, B., van Wijk, E., Gorden, N.T., et al. (2009). OFD1 is mutated in X-linked Joubert syndrome and interacts with LCA5-encoded lebercilin. Am. J. Hum. Genet. *85*, 465–481.

Corbit, K.C., Aanstad, P., Singla, V., Norman, A.R., Stainier, D.Y., and Reiter, J.F. (2005). Vertebrate smoothened functions at the primary cilium. Nature *437*, 1018–1021.

Corbit, K.C., Shyer, A.E., Dowdle, W.E., Gaulden, J., Singla, V., Chen, M.H., Chuang, P.T., and Reiter, J.F. (2008). Kif3a constrains beta-catenin-dependent Wnt signalling through dual ciliary and non-ciliary mechanisms. Nat. Cell Biol. *10*, 70–76.

Crino, P.B. (2016). The mTOR signalling cascade: paving new roads to cure neurological disease. Nat. Rev. Neurol. *12*, 379–392.

D'Gama, A.M., Geng, Y., Couto, J.A., Martin, B., Boyle, E.A., LaCoursiere, C.M., Hossain, A., Hatem, N.E., Barry, B.J., Kwiatkowski, D.J., et al. (2015). Mammalian target of rapamycin pathway mutations cause hemimegalencephaly and focal cortical dysplasia. Ann. Neurol. *77*, 720–725.

D'Gama, A.M., Woodworth, M.B., Hossain, A.A., Bizzotto, S., Hatem, N.E., LaCoursiere, C.M., Najm, I., Ying, Z., Yang, E., Barkovich, A.J., et al. (2017). Somatic mutations activating the mTOR pathway in dorsal telencephalic progenitors cause a continuum of cortical dysplasias. Cell Rep. *21*, 3754–3766.

Evsyukova, I., Plestant, C., and Anton, E.S. (2013). Integrative mechanisms of oriented neuronal migration in the developing brain. Annu. Rev. Cell Dev. Biol. *29*, 299–353.

Ferrante, M.I., Giorgio, G., Feather, S.A., Bulfone, A., Wright, V., Ghiani, M., Selicorni, A., Gammaro, L., Scolari, F., Woolf, A.S., et al. (2001). Identification of the gene for oral-facial-digital type I syndrome. Am. J. Hum. Genet. *68*, 569–576.

Fingar, D.C., Richardson, C.J., Tee, A.R., Cheatham, L., Tsou, C., and Blenis, J. (2004). mTOR controls cell cycle progression through its cell growth effectors S6K1 and 4E-BP1/eukaryotic translation initiation factor 4E. Mol. Cell. Biol. *24*, 200–216.

Foerster, P., Daclin, M., Asm, S., Faucourt, M., Boletta, A., Genovesio, A., and Spassky, N. (2017). mTORC1 signaling and primary cilia are required for brain ventricle morphogenesis. Development *144*, 201–210.

Foldvary-Schaefer, N., Bautista, J., Andermann, F., Cascino, G., and Spencer, S. (2004). Focal malformations of cortical development. Neurology *62* (*Suppl 3*), S14–S19.

Gerdes, J.M., Liu, Y., Zaghloul, N.A., Leitch, C.C., Lawson, S.S., Kato, M., Beachy, P.A., Beales, P.L., DeMartino, G.N., Fisher, S., et al. (2007). Disruption of the basal body compromises proteasomal function and perturbs intracellular Wnt response. Nat. Genet. *39*, 1350–1360.

Gleeson, J.G., and Walsh, C.A. (2000). Neuronal migration disorders: from genetic diseases to developmental mechanisms. Trends Neurosci. *23*, 352–359.

Goetz, S.C., and Anderson, K.V. (2010). The primary cilium: a signalling centre during vertebrate development. Nat. Rev. Genet. *11*, 331–344.

Guemez-Gamboa, A., Coufal, N.G., and Gleeson, J.G. (2014). Primary cilia in the developing and mature brain. Neuron *82*, 511–521.

Guo, J., Higginbotham, H., Li, J., Nichols, J., Hirt, J., Ghukasyan, V., and Anton, E.S. (2015). Developmental disruptions underlying brain abnormalities in ciliopathies. Nat. Commun. *6*, 7857.

Guschin, D.Y., Waite, A.J., Katibah, G.E., Miller, J.C., Holmes, M.C., and Rebar, E.J. (2010). A rapid and general assay for monitoring endogenous gene modification. Methods Mol. Biol. *649*, 247–256.

Higginbotham, H., Eom, T.Y., Mariani, L.E., Bachleda, A., Hirt, J., Gukassyan, V., Cusack, C.L., Lai, C., Caspary, T., and Anton, E.S. (2012). Arl13b in primary cilia regulates the migration and placement of interneurons in the developing cerebral cortex. Dev. Cell *23*, 925–938.

Higginbotham, H., Guo, J., Yokota, Y., Umberger, N.L., Su, C.Y., Li, J., Verma, N., Hirt, J., Ghukasyan, V., Caspary, T., and Anton, E.S. (2013). Arl13b-regulated cilia activities are essential for polarized radial glial scaffold formation. Nat. Neurosci. *16*, 1000–1007.

Hilgendorf, K.I., Johnson, C.T., and Jackson, P.K. (2016). The primary cilium as a cellular receiver: organizing ciliary GPCR signaling. Curr. Opin. Cell Biol. *39*, 84–92.

Hsieh, L.S., Wen, J.H., Claycomb, K., Huang, Y., Harrsch, F.A., Naegele, J.R., Hyder, F., Buchanan, G.F., and Bordey, A. (2016). Convulsive seizures from experimental focal cortical dysplasia occur independently of cell misplacement. Nat. Commun. *7*, 11753.

Jacinto, E., Loewith, R., Schmidt, A., Lin, S., Rüegg, M.A., Hall, A., and Hall, M.N. (2004). Mammalian TOR complex 2 controls the actin cytoskeleton and is rapamycin insensitive. Nat. Cell Biol. *6*, 1122–1128.

Kanamori, H., Takemura, G., Goto, K., Maruyama, R., Ono, K., Nagao, K., Tsujimoto, A., Ogino, A., Takeyama, T., Kawaguchi, T., et al. (2011). Autophagy limits acute myocardial infarction induced by permanent coronary artery occlusion. Am. J. Physiol. Heart Circ. Physiol. *300*, H2261–H2271.

Kim, H.J., Lee, H.J., Kim, H., Cho, S.W., and Kim, J.S. (2009). Targeted genome editing in human cells with zinc finger nucleases constructed via modular assembly. Genome Res. *19*, 1279–1288.

Kim, J., Lee, J.E., Heynen-Genel, S., Suyama, E., Ono, K., Lee, K., Ideker, T., Aza-Blanc, P., and Gleeson, J.G. (2010). Functional genomic screen for modulators of ciliogenesis and cilium length. Nature *464*, 1048–1051.

Kim, H., Um, E., Cho, S.R., Jung, C., Kim, H., and Kim, J.S. (2011a). Surrogate reporters for enrichment of cells with nuclease-induced mutations. Nat. Methods *8*, 941–943.

Kim, Y.H., Kang, H.C., Kim, D.S., Kim, S.H., Shim, K.W., Kim, H.D., and Lee, J.S. (2011b). Neuroimaging in identifying focal cortical dysplasia and prognostic factors in pediatric and adolescent epilepsy surgery. Epilepsia *52*, 722–727.

Kim, J., Jo, H., Hong, H., Kim, M.H., Kim, J.M., Lee, J.K., Heo, W.D., and Kim, J. (2015). Actin remodelling factors control ciliogenesis by regulating YAP/TAZ activity and vesicle trafficking. Nat. Commun. *6*, 6781.

La Fata, G., Gärtner, A., Domínguez-Iturza, N., Dresselaers, T., Dawitz, J., Poorthuis, R.B., Averna, M., Himmelreich, U., Meredith, R.M., Achsel, T., et al. (2014). FMRP regulates multipolar to bipolar transition affecting neuronal migration and cortical circuitry. Nat. Neurosci. *17*, 1693–1700.

Laplante, M., and Sabatini, D.M. (2012). mTOR signaling in growth control and disease. Cell *149*, 274–293.

Lee, J.H., and Gleeson, J.G. (2010). The role of primary cilia in neuronal function. Neurobiol. Dis. *38*, 167–172.

Lee, J.H., Huynh, M., Silhavy, J.L., Kim, S., Dixon-Salazar, T., Heiberg, A., Scott, E., Bafna, V., Hill, K.J., Collazo, A., et al. (2012a). De novo somatic mutations in components of the PI3K-AKT3-mTOR pathway cause hemimegalencephaly. Nat. Genet. *44*, 941–945.

Lee, J.H., Silhavy, J.L., Lee, J.E., Al-Gazali, L., Thomas, S., Davis, E.E., Bielas, S.L., Hill, K.J., Iannicelli, M., Brancati, F., et al. (2012b). Evolutionarily assembled cis-regulatory module at a human ciliopathy locus. Science *335*, 966–969.

Lim, K.C., and Crino, P.B. (2013). Focal malformations of cortical development: new vistas for molecular pathogenesis. Neuroscience *252*, 262–276.

Lim, J.S., Kim, W.I., Kang, H.C., Kim, S.H., Park, A.H., Park, E.K., Cho, Y.W., Kim, S., Kim, H.M., Kim, J.A., et al. (2015). Brain somatic mutations in MTOR cause focal cortical dysplasia type II leading to intractable epilepsy. Nat. Med. *21*, 395–400.

Lv, X., Jiang, H., Li, B., Liang, Q., Wang, S., Zhao, Q., and Jiao, J. (2014). The crucial role of Atg5 in cortical neurogenesis during early brain development. Sci. Rep. *4*, 6010.

May-Simera, H.L., and Kelley, M.W. (2012). Cilia, Wnt signaling, and the cytoskeleton. Cilia *1*, 7.

Mirzaa, G.M., Campbell, C.D., Solovieff, N., Goold, C., Jansen, L.A., Menon, S., Timms, A.E., Conti, V., Biag, J.D., Adams, C., et al. (2016). Association of MTOR mutations with developmental brain disorders, including megalencephaly, focal cortical dysplasia, and pigmentary mosaicism. JAMA Neurol. *73*, 836–845.

Mizushima, N., Noda, T., Yoshimori, T., Tanaka, Y., Ishii, T., George, M.D., Klionsky, D.J., Ohsumi, M., and Ohsumi, Y. (1998). A protein conjugation system essential for autophagy. Nature *395*, 395–398.

Mizushima, N., Yamamoto, A., Hatano, M., Kobayashi, Y., Kabeya, Y., Suzuki, K., Tokuhisa, T., Ohsumi, Y., and Yoshimori, T. (2001). Dissection of autophagosome formation using Apg5-deficient mouse embryonic stem cells. J. Cell Biol. *152*, 657–668.

Møller, R.S., Weckhuysen, S., Chipaux, M., Marsan, E., Taly, V., Bebin, E.M., Hiatt, S.M., Prokop, J.W., Bowling, K.M., Mei, D., et al. (2016). Germline and somatic mutations in the *MTOR* gene in focal cortical dysplasia and epilepsy. Neurol. Genet. *2*, e118.

Munji, R.N., Choe, Y., Li, G., Siegenthaler, J.A., and Pleasure, S.J. (2011). Wnt signaling regulates neuronal differentiation of cortical intermediate progenitors. J. Neurosci. *31*, 1676–1687.

Nakagawa, N., Li, J., Yabuno-Nakagawa, K., Eom, T.Y., Cowles, M., Mapp, T., Taylor, R., and Anton, E.S. (2017). APC sets the Wnt tone necessary for cerebral cortical progenitor development. Genes Dev. *31*, 1679–1692.

Nakashima, M., Saitsu, H., Takei, N., Tohyama, J., Kato, M., Kitaura, H., Shiina, M., Shirozu, H., Masuda, H., Watanabe, K., et al. (2015). Somatic mutations in the MTOR gene cause focal cortical dysplasia type IIb. Ann. Neurol. *78*, 375–386.

Nigg, E.A., and Stearns, T. (2011). The centrosome cycle: Centriole biogenesis, duplication and inherent asymmetries. Nat. Cell Biol. *13*, 1154–1160.

Palmini, A., and Holthausen, H. (2013). Focal malformations of cortical development: a most relevant etiology of epilepsy in children. Handb. Clin. Neurol. *111*, 549–565.

Ramakrishna, S., Cho, S.W., Kim, S., Song, M., Gopalappa, R., Kim, J.S., and Kim, H. (2014a). Surrogate reporter-based enrichment of cells containing RNA-guided Cas9 nuclease-induced mutations. Nat. Commun. *5*, 3378.

Ramakrishna, S., Kwaku Dad, A.B., Beloor, J., Gopalappa, R., Lee, S.K., and Kim, H. (2014b). Gene disruption by cell-penetrating peptide-mediated delivery of Cas9 protein and guide RNA. Genome Res. *24*, 1020–1027.

Reiter, J.F., and Leroux, M.R. (2017). Genes and molecular pathways underpinning ciliopathies. Nat. Rev. Mol. Cell Biol. *18*, 533–547.

Saitsu, H., Sonoda, M., Higashijima, T., Shirozu, H., Masuda, H., Tohyama, J., Kato, M., Nakashima, M., Tsurusaki, Y., Mizuguchi, T., et al. (2016). Somatic mutations in GLI3 and OFD1 involved in sonic hedgehog signaling cause hypothalamic hamartoma. Ann. Clin. Transl. Neurol. *3*, 356–365.

Sarbassov, D.D., Ali, S.M., Kim, D.H., Guertin, D.A., Latek, R.R., Erdjument-Bromage, H., Tempst, P., and Sabatini, D.M. (2004). Rictor, a novel binding partner of mTOR, defines a rapamycin-insensitive and raptor-independent pathway that regulates the cytoskeleton. Curr. Biol. *14*, 1296–1302.

Schwartzkroin, P.A., and Walsh, C.A. (2000). Cortical malformations and epilepsy. Ment. Retard. Dev. Disabil. Res. Rev. *6*, 268–280.

Sharma, N., Kosan, Z.A., Stallworth, J.E., Berbari, N.F., and Yoder, B.K. (2011). Soluble levels of cytosolic tubulin regulate ciliary length control. Mol. Biol. Cell *22*, 806–816.

Singla, V., Hunkapiller, J., Santos, N., Seol, A.D., Norman, A.R., Wakenight, P., Skarnes, W.C., and Reiter, J.F. (2010a). Floxin, a resource for genetically engineering mouse ESCs. Nat. Methods *7*, 50–52.

Singla, V., Romaguera-Ros, M., Garcia-Verdugo, J.M., and Reiter, J.F. (2010b). Ofd1, a human disease gene, regulates the length and distal structure of centrioles. Dev. Cell *18*, 410–424.

Suzuki, K., Kirisako, T., Kamada, Y., Mizushima, N., Noda, T., and Ohsumi, Y. (2001). The pre-autophagosomal structure organized by concerted functions of APG genes is essential for autophagosome formation. EMBO J. *20*, 5971–5981.

Tabata, H., and Nakajima, K. (2001). Efficient in utero gene transfer system to the developing mouse brain using electroporation: Visualization of neuronal migration in the developing cortex. Neuroscience *103*, 865–872.

Tang, Z., Lin, M.G., Stowe, T.R., Chen, S., Zhu, M., Stearns, T., Franco, B., and Zhong, Q. (2013). Autophagy promotes primary ciliogenesis by removing OFD1 from centriolar satellites. Nature *502*, 254–257.

Ventura, A., Meissner, A., Dillon, C.P., McManus, M., Sharp, P.A., Van Parijs, L., Jaenisch, R., and Jacks, T. (2004). Cre-lox-regulated conditional RNA interference from transgenes. Proc. Natl. Acad. Sci. USA *101*, 10380–10385.

Wang, S., Li, B., Qiao, H., Lv, X., Liang, Q., Shi, Z., Xia, W., Ji, F., and Jiao, J. (2014). Autophagy-related gene Atg5 is essential for astrocyte differentiation in the developing mouse cortex. EMBO Rep. *15*, 1053–1061.

Wegiel, J., Kuchna, I., Nowicki, K., Imaki, H., Wegiel, J., Marchi, E., Ma, S.Y., Chauhan, A., Chauhan, V., Bobrowicz, T.W., et al. (2010). The neuropathology of autism: Defects of neurogenesis and neuronal migration, and dysplastic changes. Acta Neuropathol. *119*, 755–770.

Yasin, S.A., Ali, A.M., Tata, M., Picker, S.R., Anderson, G.W., Latimer-Bowman, E., Nicholson, S.L., Harkness, W., Cross, J.H., Paine, S.M., and Jacques, T.S. (2013). mTOR-dependent abnormalities in autophagy characterize human malformations of cortical development: evidence from focal cortical dysplasia and tuberous sclerosis. Acta Neuropathol. *126*, 207–218.

Zeng, L.H., Xu, L., Gutmann, D.H., and Wong, M. (2008). Rapamycin prevents epilepsy in a mouse model of tuberous sclerosis complex. Ann. Neurol. *63*, 444–453.

STAR★METHODS

KEY RESOURCES TABLE

REAGENT or RESOURCE	SOURCE	IDENTIFIER
Antibodies		
rabbit polyclonal anti-Arl13b	Proteintech	Cat#17711-1-AP; RRID: AB_2060867
rabbit polyclonal anti-p62	MBL	Cat#PM045; RRID: AB_1279301
mouse monoclonal anti-acetylated tubulin	Sigma	Cat#T7451; RRID: AB_609894
rabbit polyclonal anti-OFD1	gift from J.F.R	N/A
mouse monoclonal anti-polyglutamylated tubulin	Adipogen	Cat# AG-20B-0020; RRID: AB_2490210
mouse monoclonal anti-γ tubulin	Sigma	Cat#T6557; RRID: AB_477584
rabbit polyclonal anti-Ki67	Abcam	Cat# ab15580; RRID: AB_443209
mouse monoclonal anti-NeuN	Merck Millipore	Cat#MAB377; RRID: AB_2298772
rabbit monoclonal anti-phosphorylated S6 ribosomal protein	Cell Signaling Technology	Cat#5364; RRID: AB_10694233
rabbit polyclonal anti-CDP(cux1)	Santa Cruz Biotechnology	Cat#sc-13024; RRID: AB_2261231
Rabbit polyclonal anti-Ctip2	Abcam	Cat#ab28448;RRID: AB_1140055
Rabbit polyclonal anti-Tbr1	Abcam	Cat#ab31940; RRID: AB_2200219
rabbit polyclonal anti-ACIII(C-20)	Santa Cruz Biotechnology	Cat#sc-588; RRID: AB_630839
rabbit polyclonal anti-p62/SQSTM1	MBL	Cat#PM045; RRID: AB_1279301
rabbit polyclonal anti-Atg5	Novus Biologicals	Cat#NB110-53818; RRID: AB_828587
rabbit monoclonal anti-S6 ribosomal protein	Cell Signaling Technology	Cat#2217; RRID: AB_331355
mouse monoclonal anti-α tubulin	Sigma	Cat#T6074; RRID: AB_477582
rabbit polyclonal anti-LC3	Novus Biologicals	Cat# NB100-2220; RRID: AB_10003146
rabbit monoclonal anti-Myc	Cell Signaling Technology	Cat#2276; RRID: AB_331783
mouse monoclonal anti-Flag	Cell Signaling Technology	Cat#8146; RRID: AB_10950495
rabbit polyclonal anti-PH3	Abcam	Cat#5176; RRID: AB_304763
rat anti-BrdU	Abcam	Cat#6326; RRID: AB_305426
Chemicals, Peptides, and Recombinant Proteins		
Cytochalasin D	Sigma	Cat#C2618; CAS: 22144-77-0
Chloroquine	Sigma	Cat#C6628; CAS: 50-63-5
Rapamycin	Merck Millipore	Cat#553210; CAS: 53123-88-9
Torin-1	Merck Millipore	Cat#475991; CAS: 1222998-36-8
Rapamycin	LC labs	CAS: 53123-88-9
Critical Commercial Assays		
K-LISA mTOR activity kit	Calbiochem	CBA055
Experimental Models: Cell Lines		
mouse ; NIH/3T3	ATCC	CRL-1658; RRID: CVCL_0594
mouse ; genome-edited MTOR p.Cys1483Tyr NIH/3T3	This paper	N/A
human ; HEK293T	ATCC	CRL-3216; RRID: CVCL_0063
Experimental Models: Organisms/Strains		
Mouse: CD-1 wild-type	DBL	N/A
Mouse: C57BL/6 wild-type	DBL	N/A
Oligonucleotides		
Primers for *MTOR* c.4448G > A validation by Sanger sequencing in patient DNA: forward CCTCACAGCA GTCTTTCTTTCC	This paper	N/A
Primers for *MTOR* c.4448G > A validation by Sanger sequencing in patient DNA: reverse CATGCCATCAT TCTAGGAAGC	This paper	N/A

(*Continued on next page*)

Continued

REAGENT or RESOURCE	SOURCE	IDENTIFIER
Primer for mutagenesis: MTOR p.Cys1483Tyr: forward GCCGCATGCGCTACCTCGAGGCC	This paper	N/A
Primer for mutagenesis: MTOR p.Cys1483Tyr: reverse GGCCTCGAGGTAGCGCATGCGGC	This paper	N/A
Oligonucleotides used for generation of MTOR p.Cys1483Tyr genome-edited NIH/3T3 cell line	Table S2	N/A
Primers for subcloning Ofd1 knockdown sequence into pCIG-MTOR p.Cys1483Tyr-IRES-EGFP plasmid: forward CAGAGGCCGAGGCCGCCTCGGCCCACTATAGG	This paper	N/A
Primers for subcloning Ofd1 knockdown sequence into pCIG-MTOR p.Cys1483Tyr-IRES-EGFP plasmid: reverse ATAGCTCAGAGGCCGAGGCGGCCGTGACAC	This paper	N/A
shRNA targeting sequence: mouse *Atg5*: GGACTGCA GAATGACAGAT	Kanamori et al., 2011	N/A
shRNA targeting sequence: scrambled: GGAATCTCA TTCGATGCAT	This paper	N/A
shRNA clonal set targeting mouse *Ofd1*	QIAGEN	Cat#km34866G
Recombinant DNA		
Plasmid: pCIG-MTOR wild-type-IRES-EGFP	Lim et al., 2015	N/A
Plasmid: pCIG-MTOR p.Cys1483Tyr-IRES-EGFP	This paper	N/A
Plasmid: pCIG-MTOR p.Leu2427Pro-IRES-EGFP	Lim et al., 2015	N/A
Plasmid: pIRES2-eGFP-OFD1-Myc	Singla et al., 2010a	Addgene Plasmid #24560
Plasmid: mouse *Ofd1* shRNA clonal set	QIAGEN	Cat#km34866G
Plasmid: pCIG-MTOR p.Cys1483Tyr-IRES-EGFP with scrambled shRNA	This paper	N/A
Plasmid: pCIG-MTOR p.Cys1483Tyr-IRES-EGFP with *Ofd1* shRNA	This paper	N/A
Plasmid: pSicoR	Ventura et al., 2004	Addgene Plasmid #11579
Plasmid: Cas9-2A-RFP-2A-PAC	Toolgen	N/A
Plasmid: sgRNA	Toolgen	N/A
Plasmid: pCIG-Wnt5a-IRES-tdTomato	This paper	N/A
Plasmid: M38 TOP-dGFP	Randall Moon	Addgene Plasmid #17114
Plasmid:pCLX-CHOP-dGFP	Boitard et al., 2015	Addgene Plasmid #71299
Software and Algorithms		
SureDesign online tool	Agilent technologies	https://www.genomics.agilent.com/en/NGS-Design-Tools/SureDesign-Custom-Design-Tool/?cid=AG-PT-155&tabId=AG-PR-1198
GATK "best practice" pipeline	BROAD institute	https://software.broadinstitute.org/gatk/
Burrows-Wheeler aligner (BWA)	BROAD institute	https://software.broadinstitute.org/gatk/
MuTect	BROAD institute	https://software.broadinstitute.org/gatk/
SnpEff	Cingolani et al., 2012	http://snpeff.sourceforge.net/index.html
FIJI (ImageJ)	NIH	ImageJ Version 2
Image Lab	Bio-Rad	Version 5.2
GraphPad Prism	GraphPad Software	https://www.graphpad.com/scientific-software/prism/
Neurolucida	MBF Bioscience	http://www.mbfbioscience.com/neurolucida

CONTACT FOR REAGENT AND RESOURCE SHARING

Further information and requests for resources and reagents should be directed to and will be fulfilled by the Lead Contact, Jeong Ho Lee (jhlee4246@kaist.ac.kr).

EXPERIMENTAL MODEL AND SUBJECT DETAILS

Subject ascertainment

Individuals with focal malformation of cortical development (FMCD), including FCD, TSC, and HME, who had undergone epilepsy surgery were identified through Severance Children's Hospital. Enrolled individuals met the study entry criteria for FMCD and underwent the extensive presurgical evaluations, including video-electroencephalography (EEG) monitoring, high-resolution MRI fluorodeoxyglucose (FDG)-PET, and subtraction ictal single-photon emission computed tomography (SPECT) co-registered to MRI (SISCOM) to localize anatomic lesions. The presurgical and surgical protocols have been published previously (Kim et al., 2011b; Lim et al., 2015). The resection margin for epilepsy of the neocortical origin was defined by (i) the presence of a massive and exclusive ictal-onset zone confirmed by intracranial EEG; (ii) various interictal intracranial EEG findings including > 3/s repetitive spikes, runs of repetitive spike and slow wave discharges, localized or spindle-shaped fast activities, and electrodecremental fast activities; and (iii) the absence of the eloquent cortex. Complete resection was defined by resection of all areas with seizure-onset and irritative zones on intracranial EEG. The pathological diagnosis of the patients with FCDII was reconfirmed for this study. Non-FMCD brain specimen was collected from resection margin for epilepsy of an individual with Lennox-Gastaut syndrome (LGS). Clinical and molecular genetic information of individuals enrolled in this study is listed in Table S1. Sample size was not predetermined. The study was performed and all human tissues were obtained in accordance with protocols approved by Severance Hospital and KAIST Institutional Review Board and Committee on Human Research. Informed consent from the parent of individuals with FMCD was obtained.

Animals

C57BL/6 or CD-1 mice (DBL, Korea) were used in experiments without sex discrimination, and they were housed in isolator cages with free access to food and water that were located in a room maintained at a constant temperature of 23°C on a 12-h light-dark cycle with lights off at 7:00 p.m. All of the mice used in this study were healthy mice with normal immune status and they were not involved in any previous test or drug treatment. All procedures were approved by KAIST Institutional Animal Care and Use Committee.

Cell culture

HEK293T cell line (ATCC, USA) was cultured in DMEM (LM 001-05, Welgene, Korea) supplemented with 10% FBS (PK004-07, Welgene, Korea) and 1% penicillin/streptomycin at 37°C and 5% CO_2. NIH/3T3 wild-type (ATCC, USA) and genome-edited MTOR p.Cys1483Tyr cell lines were cultured in DMEM (LM 001-05, Welgene, Korea) supplemented with 10% Bovine serum (16170078, Thermo, USA) and 1% penicillin/streptomycin at 37°C and 5% CO_2. All cell lines tested negative for mycoplasma contamination, but have not been further authenticated. For western blot analysis and immunofluorescence, cells were seeded at 6-well plate (3506, Corning, USA) and 4-chambered slide (154917, Thermo, USA), respectively. To induce primary ciliogenesis, cells were incubated in serum-free DMEM for 24 hours after wash with serum-free DMEM. For plasmid DNA transient transfection, we used iN-fect *in vitro* transfection reagent (15081, Intron, Korea) according to manufacturer's protocol.

METHOD DETAILS

Targeted hybrid capture sequencing and bioinformatic analysis

Targeted hybrid capture sequencing was performed as previously described (Lim et al., 2015). In brief, we designed hybrid capture probe including *MTOR* using SureDesign online tools (Agilent Technologies). Target capture was carried out according to the manufacturer's protocol (Agilent Technologies). Then, we generated analysis-ready bam file using GATK "Best Practice" pipeline (BROAD institute). We aligned raw sequence from fastq file to the hg19/GRCh37 assembly of the human genome reference sequence using Burrows-Wheeler aligner (BWA) (BROAD institute). To identify *de novo* single nucleotide variants (SNVs) in brain sample, we utilized the MuTect algorithm (BROAD institute) which is designed for analyzing blood-brain paired sequencing datasets. We annotated identified variants with SnpEff program (Cingolani et al., 2012). We then excluded 1) mutations with a mutant read < 4, allele frequency < 1% and total read depth < 100 × to remove erroneous calls; 2) mutations with a putative low impact score; 3) mutations with a PolyPhen score < 0.9 and phastCons score < 0.9; and 4) mutations with allele frequency in ExAC database of east Asian population > 0.1%.

Plasmids

pcDNA3.1 Flag- tagged MTOR p.Cys1483Tyr plasmid and pCIG-MTOR p.Cys1483Tyr-IRES-EGFP plasmid were generated from MTOR wild-type inserted plasmid by site-directed mutagenesis described below in detail. Plasmids containing shRNA against

mouse *Ofd1* transcript and scrambled shRNA were purchased from QIAGEN (SureSilencing shRNA plasmid for mouse *Ofd1*) (km34866G, QIAGEN, USA). To estimate knockdown efficiency of *Ofd1* shRNA, a pCIG-Ofd1:Myc-IRES-EGFP plasmid (24560, Addgene) (Singla et al., 2010a) was co-transfected with *Ofd1* shRNA at HEK293T cell. To insert the sequence corresponding to *Ofd1* knockdown (from U1 promoter start site to U1 termination site) into pCIG-MTOR p.Cys1483Tyr-IRES-EGFP plasmid, we utilized a restriction enzyme site for *SfiI*. The PCR fragments corresponding to sequences from scrambled shRNA or *Ofd1* shRNA were inserted into the *SfiI* site of the pCIG-MTOR p.Cys1483Tyr-IRES-GFP plasmid using primer pairs, SfiI-U1-F; 5′-CAGAGGCC GAGGCCGCCTCGGCCCACTATAGG-3′ and SfiI-U1-R; 5′-ATAGCTCAGAGGCCGAGGCGGCCGTGACAC-3′, resulting in the plasmid pCIG-MTOR p.Cys1483Tyr-IRES-EGFP with scrambled shRNA or *Ofd1* shRNA. shRNA oligonucleotides against mouse *Atg5* transcript (5′- GGACTGCAGAATGACAGAT-3′) and scrambled shRNA sequence (5′-GGAATCTCATTCGATGCAT-3′) were inserted into pSicoR-GFP plasmid (11579, Addgene) (Ventura et al., 2004). The sequence for *Atg5* shRNA was described previously (Kanamori et al., 2011). To examine the Wnt signaling pathway, Wnt signaling-dependent reporter construct including M38 TOP-dGFP (17114, Addgene) and pCLX-CHOP-dGFP (71299, Addgene) were used with pCIG-MTOR wild-type or p.Cys1483Tyr-IRES-tdTomato and pCIG-empty or Wnt5a-IRES-tdTomato plasmids.

Mutagenesis and cloning of MTOR mutant construct

pcDNA3.1 Flag- tagged MTOR wild-type construct was kindly provided by K.-L. Guan at UCSD. This construct was used to generate MTOR p.Cys1483Tyr vector with a QuikChange II site-directed mutagenesis kit (200523, Stratagene, USA). The primers for mutagenesis are as follows, sense; 5′-GCCGCATGCGCTACCTCGAGGCC-3′ and antisense; 5′-GGCCTCGAGGTAGCGCATGCGGC-3′. For generating pCIG-MTOR p.Cys1483Tyr-IRES-GFP vector, we utilized pCIG2- C1 (modified from pCIG2) vector which was previously described (Lim et al., 2015). Briefly, the annealed primer set (forward; 5′-AATTCCAATTGCCC GGGCTTAAGATCGATACGCGTA-3′ and reverse; 5′-CCGGTACGC GTATCGATCTTAAGCCCGGGCAATTGG-3′) was inserted into the EcoRI and XmaI of pCIG2 (CAG promoter-MCS-IRES-EGFP) to generate pCIG2- C1 with new restriction enzyme sites, *MfeI* and *MluI*. The PCR fragments corresponding to p.Cys1483Tyr mutated *MTOR* genes were subcloned into the *MfeI* and *MluI* sites of the pCIG2-C1 vector using the primer pairs, MTOR-MfeI-flag-F; 5′-GATCACAATTGTGGCCACCATGGACTACAAGGACGACGATGACAAGATGC-3′ and MTOR-MluI-R; 5′-TGATCAACGCGTTTACCAGAAAGGGCACCAGCCAATATAGC-3′, resulting in the plasmid pCIG-MTOR p.Cys1483Tyr-IRES-EGFP.

Cas9 and guide RNA constructs

For screening of sgRNAs, we used a plasmid encoding Cas9-2A-mRFP-2A-PAC (Puromycin N-acetyl-transferase, puromycin resistance gene) and a plasmid encoding sgRNAs, both of which are from Toolgen (Seoul, South Korea). The sgRNA target sequences were manually designed based on PAM motif sequence (NGG) near the *Mtor* c.4448G and cloned into the vectors as previously described (Ramakrishna et al., 2014a). Briefly, oligonucleotides containing each target sequence were synthesized (Bioneer, Seoul, South Korea) and annealed *in vitro* using a thermocycler. The vector was digested with *BsaI* restriction enzyme and ligated with the annealed oligonucleotides. Oligonucleotide sequences are listed in Table S2.

T7E1 assay

NIH/3T3 cells were co-transfected with plasmids encoding Cas9 and sgRNA targeting *Mtor* c.4448G site at a 1:2 weight ratio using Neon (Thermo, USA) according to the manufacturer's instructions. Three days after transfection, cells were subjected to the T7 endonuclease 1 (T7E1) assay. The T7E1 assay was performed as previously described (Kim et al., 2009, 2011a). Genomic DNA was isolated using the Wizard Genomic DNA purification Kit (A1120, Promega, USA) according to the manufacturer's instructions. The region including the nuclease target site was nested PCR-amplified using primer pairs, forward; 5′-TGCATTAAGAATGCGGAGAA-3′, reverse; 5′-AGGGTCACATGGCTCTTCTG-3′. The amplicons were denatured by heating and annealed to allow heteroduplex DNA formation, which was treated with 5 units of T7 endonuclease 1 (M0302, NEB, USA) for 20 minutes at 37°C followed by analysis using 2% agarose gel electrophoresis. Mutation frequencies were calculated as previously described based on the band intensities using ImageJ software and the following equation (Guschin et al., 2010): mutation frequency (%) = $100 \times (1 - (1 - \text{fraction cleaved})^{1/2})$, where the fraction cleaved is the total relative density of the cleavage bands divided by the sum of the relative density of the cleavage bands and uncut bands.

Preparation of single-stranded oligodeoxynucleotides (ssODN)

A KpnI restriction enzyme site was incorporated at the desired point mutation region for screening homology-directed repair-mediated mutated clones by Restriction Fragment Length Polymorphism (RFLP) assay. The ssODN donor template (5′-CAAACAAGGAA GACCCGGAGCTGATGCTGGGCCGAATGCGGTACCTCGAAGCCTTGGGGGAATGGTGAGCTTCACTGGAGTGATGACCTG-3′) was synthesized and purified by PAGE (Bioneer, South Korea). ssODN was diluted with RNase free water to 100 μM, divided into aliquots and stored at −20°C. ssODN was electroporated into NIH/3T3 cells using the NEON transfection system (Thermo, USA).

Generation of knock-in clones

NIH/3T3 cell was co-transfected with plasmid encoding Cas9, sgRNA targeting *Mtor* c.4448G and ssODN donor DNA. Cas9 encoding plasmid and sgRNA were transfected at a 1:2 weight ratio using Neon. In the case of ssODN donor DNA, 500 pmol of ssODN is

used per reaction. One day after transfection, cells were subjected to puromycin selection (1μg/mL) for three days. Then, cells were trypsinized and resuspended in DMEM medium and seeded into 96-well plates at an average density of 0.25 cells/well. Twenty days after the cell seeding, each well was microscopically evaluated and single cell-derived round colonies were selected (Ramakrishna et al., 2014b). Each selected colony was individually trypsinized and replated into 24-well plates. Six days after the subculture, genomic DNA was isolated from each clone and subjected to the RFLP analysis and Sanger sequencing. Single-cell derived knock-in clones are screened by performing genomic DNA and subjected to PCR amplification with primers flanking the target site, forward; 5′-CTTCACCACGTGCTCTCAGT-3′, reverse; 5′-GGCTCACAGCCCCAATTCTACT-3′. PCR amplicons were digested with KpnI. Sequencing of the genomic region including the target sequence was performed as previously described (Kim et al., 2011a; Ramakrishna et al., 2014a). Briefly, PCR amplicons that included nuclease target sites were cloned into the T-Blunt vector (Promega, USA) and the cloned plasmids were sequenced using the M13 Forward primer (5′-GTAAAACGACGGCCAGT-3′).

Pharmacological studies

To see whether MTOR p.Cys1483Tyr mutation influences stability of actin cytoskeleton, we treated 100nM cytochalasin D (CytD) (C2618, Sigma, USA) resuspended in dimethyl sulfoxide (DMSO) in cells with media containing 10% bovine serum for 24 hours. To inhibit autophagy, we treated 20uM chloroquine (C6628, Sigma, USA), an inhibitor for autophagy, in cells with serum-free media for 24 hours. To inhibit the MTOR kinase activity, we treated 200nM rapamycin (553210, Calbiochem, USA) or 200nM torin-1 (475991, Merck Millipore, USA) in cells with serum-free media for 24 hours.

In vitro MTOR kinase assay

In vitro MTOR kinase assay was performed as previously described (Lim et al., 2015). The kinase activity of MTOR was assayed using a K-LISA mTOR activity kit (CBA055, Calbiochem, USA) according to the manufacturer's protocol. Briefly, transfected cells were lysed with TBS containing 1% Tween 20 and Halt protease and phosphatase inhibitor cocktail (78440, Thermo Scientific, USA). 1mg of total lysate was pre-cleared by adding 15 μl of protein G beads (10004D, Life technologies, USA) and incubated for 15 minutes at 4°C. Anti-Flag antibodies (8146, Cell signaling Technology, USA, 1/250 dilution) were added to the pre-cleared lysate and incubated overnight at 4°C. Then, 50 μl of protein G beads were added and incubated for 90 minutes at 4°C. The supernatant was carefully discarded. The pelleted beads were washed 4 times with 500 μl of lysis buffer and 1 time with 1 × kinase buffer supplied with the K-LISA mTOR activity kit. The pelleted beads were resuspended in 50 μl of 2 × kinase buffer and 50 μl of mTOR substrate (p70S6K-GST fusion protein), followed by incubation for 30 minutes at 30°C. The reaction mixture was incubated in a glutathione-coated 96-well plate and incubated for 30 minutes at 30°C. The phosphorylated substrate was detected using anti-p70S6K-T389 antibody (JA9357, Merck Millipore, Germany, 1/1,000 dilution), HRP antibody- conjugate and TMB substrate. Relative fluorescence intensities were measured by reading the absorbance at 450 nm.

Laser-capture microdissection with the subsequent Sanger sequencing

Laser-capture microdissection with the subsequent Sanger sequencing for validation of *MTOR* c.4448G > A mutation was performed as previously described (Lim et al., 2015). Briefly, freshly frozen brain sample was fixed in phosphate-buffered 4% paraformaldehyde for overnight at 4°C. The next day, fixed tissue was submerged in 30% sucrose for cryoprotection at 4°C until they settle down to bottom. Cryoprotected tissue was embedded in gelatin block (7.5% gelatin in 10% sucrose/PB) and stored at −80°C. Cryostat-cut sections (10 μm thick) were collected and placed on glass slides. After immunostaining for phosphorylated S6 and NeuN, phosphorylated S6-immunoreactive cytomegalic neurons (n = ∼40) were microdissected with PALM laser capture system (Carl Zeiss, Germany) and collected in the adhesive cap (Carl Zeiss, Germany). Genomic DNA was extracted from collected neurons using QiAamp DNA microkit under manufacturer's isolation of genomic DNA from LCM tissues (QIAGEN, USA). Genomic DNA extracted from phosphorylated S6-immunoreactive cytomegalic neurons was used for validating *MTOR* c.4448G > A mutation. This region was amplified by PCR using targeted primer set and high-fidelity PrimeSTAR GXL DNA polymerase (Takara, Japan). The detailed sequence of the primer set is as follows: forward; 5′-CCTCACAGCAGTCTTTCTTTCC-3′ and reverse; 5′-CATGCCATCATTCTAG GAAGC-3′. Amplified PCR product was purified with MEGA quick spin total fragment DNA purification kit (Intron, Korea). Then, we performed Sanger sequencing (Cosmogenetech, Korea) with above forward PCR primer; 5′-CCTCACAGCAGTCTTTCTTTCC-3′.

Western blot analysis

Protein lysates from cells were prepared with 1% Triton X-100 in PBS with Halt protease and phosphatase inhibitor cocktail (78440, Thermo Scientific, USA). Protein lysates from GFP-expressing cortical regions of mice embryo (E16) were prepared by homogenizing tissue in lysis buffer (1% Triton X-100, 0.1% SDS, 0.5% Na-deoxycholate, 0.1 M NaCl, 1% NP-40 in 10 mM HEPES). After lysis for 30 minutes at 4°C, they were centrifuged at 13000 rpm for 30 minutes. Supernatants were used for measuring the protein concentration by Pierce BCA assay kit (23225, Thermo, USA). Proteins were resolved by SDS-PAGE and transferred to PVDF membranes (Millipore, USA). The membranes were blocked with 5% BSA (Bovogen, Australia) in TBS containing 0.1% Tween 20 (TBST) for 1 hour at room temperature. They were incubated with diluted primary antibodies including rabbit anti-phosphorylated S6 ribosomal protein (5364, Cell Signaling Technology, USA), rabbit anti-S6 ribosomal protein (2217, Cell Signaling Technology, USA), mouse anti-α tubulin (T6074, Sigma, USA), mouse anti-Flag (8146, Cell Signaling Technology, USA), rabbit anti-OFD1 (gift from Jeremy F. Reiter), rabbit anti-LC3 (NB100-2220, Novus Biologicals, USA), rabbit anti-p62 (PM045, MBL, USA), rabbit anti-Atg5 (NB110-53818, Novus

Biologicals, USA) and mouse anti-Myc (2276, Cell Signaling Technology, USA) at 4°C overnight. The next day, the membranes were washed 4 times with TBST for each 10 minutes at room temperature. After washing, they were incubated with diluted secondary antibodies including HRP linked anti-rabbit (7074, Cell Signaling Technology, USA) and HRP linked anti-mouse (7076, Cell Signaling Technology, USA) for 2 hours at room temperature. After washing 4 times with TBST for each 10 minutes at room temperature, immunodetection was performed using ECL reaction reagents.

In utero electroporation and BrdU injection

Timed pregnant CD-1 or C57BL/6 mice (E14) were anesthetized with isoflurane (0.4 L/min of oxygen and isoflurane vaporizer gauge 3.5 during surgery operation). Each DNA plasmids were extracted with EndoFree Plasmid Maxi kit (12362, QIAGEN, USA). The uterine horn was exposed, and 1 μl of endotoxin-free plasmids (2 μg/μl) including 0.2% Fast green (F7252, Sigma, USA) per embryo were injected into one side of lateral ventricle using pulled glass capillary. Injected plasmids were electroporated on the head of the embryo by discharging 50 V with the ECM830 electroporator (BTX-Harvard apparatus) in five electric pulses of 100 ms at 900 ms intervals. For cell cycle analysis, BrdU (Bromodeoxyuridine) (100mg/kg) was injected intraperitoneally 2 hours before brain preparation (E16).

Video-Electroencephalography (EEG) monitoring

EEG signals from the epidural electrodes located on frontal lobes (AP + 2.8 mm, ML ± 1.5 mm) and temporal lobes (AP - 2.4 mm, ML ± 2.4 mm) were recorded using cerebellum as a reference. More than 4 days of recovery from the surgery, EEG signals were recorded for 2∼5 ds (6 h/d). Signals were amplified with GRASS model 9 EEG/Polysomnograph (GRASS technologies, USA), recorded with Digidata 1320A (Molecular Devices, USA), and analyzed with pCLAMP program (Molecular Devices, USA).

In vivo rapamycin treatment

Rapamycin was treated as previously described (Lim et al., 2015; Zeng et al., 2008). In brief, rapamycin (LC Labs, USA) was dissolved initially in 100% ethanol to 20 mg/ml stock solution, stored at −20°C. Immediately before injection, the stock solution was diluted in 5% polyethyleneglycol 400 and 5% Tween 80 to final concentrations of 1 mg/ml rapamycin and 4% ethanol. After observing spontaneous seizures using video recordings and electroencephalography (EEG) recordings, the mice were injected daily through intraperitoneal route with 10 mg/kg rapamycin, or vehicle alone for 2 weeks.

Immunocytochemistry and image analysis

Cells were washed with cold PBS, followed by methanol fixation for 5 minutes at −20°C. After washing methanol with PBS, they were blocked with 10% goat serum in PBS for 1 hour at room temperature. They were incubated overnight at 4°C with the following primary antibodies: rabbit anti-Arl13b (17711-1-AP, Proteintech, USA), rabbit anti-p62 (PM045, MBL, USA), mouse anti-acetylated tubulin (T7451, Sigma, USA), rabbit anti-OFD1 (gift from Jeremy F. Reiter), mouse anti-polyglutamylated tubulin (AG-20B-0020, Adipogen, USA), mouse anti-γ tubulin (T6557, Sigma, USA), and rabbit anti-Ki67 (ab15580, Abcam, USA). The next day, cells were washed 3 times with PBS for 5 minutes each. After washing, they were incubated 1 hour at room temperature with the following secondary antibodies: Alexa Fluor 555-conjugated goat antibody to mouse (A21422, Thermo Scientific, USA), Alexa Fluor 488-conjugated goat antibody to mouse (A11001, Thermo Scientific, USA), Alexa Fluor 555-conjugated goat antibody to rabbit (A21428, Thermo Scientific, USA), and Alexa Fluor 488-conjugated goat antibody to rabbit (A11008, Thermo Scientific, USA). After incubation, the cells were washed 3 times with PBS for 5 minutes each. The cells were mounted with prolong gold antifade reagent with DAPI (P36931, Thermo Scientific, USA). Images were acquired using a Delta Vision Spectris Imaging System (Applied Precision) and analyzed using ImageJ software (https://imagej.nih.gov/ij).

Immunohistochemistry and image analysis

Brains of E16, E18 mice were harvested and fixed with phosphate-buffered 4% paraformaldehyde at 4°C overnight. The next day, brains were submerged in 30% sucrose for cryoprotection at 4°C until they settle down to bottom. Cryoprotected brains were embedded in gelatin block (7.5% gelatin in 10% sucrose/PB) and stored at −80°C. Brains of adult mice (> P56) were harvested after transcardiac perfusion with phosphate-buffered 4% paraformaldehyde. Then, they were post-fixed with 4% PFA at 4°C overnight. The next day, brains were submerged in 30% sucrose for cryoprotection at 4°C until they settle down to bottom. Cryoprotected brains were embedded in gelatin block (7.5% gelatin in 10% sucrose/PB) and stored at −80°C. For the patient sample, freshly frozen tissues were fixed with phosphate-buffered 4% paraformaldehyde at 4°C overnight. The next day, brains were submerged in 30% sucrose for cryoprotection at 4°C until they settle down to bottom. Cryoprotected brains were embedded in gelatin block (7.5% gelatin in 10% sucrose/PB) and stored at −80°C. Cryostat-cut sections (20 μm thickness) were collected and placed on glass slides. For the cilia staining in patient brain tissues, sections were treated with 1% SDS for 5 min at room temperature before blocking. Sections were blocked with PB-GT (0.2% gelatin, 0.1% Triton X-100 in PBS) for 1 hour at room temperature. They were incubated overnight at 4°C with the following primary antibodies: mouse anti-NeuN (MAB377, Merck Millipore, Germany), rabbit anti-phosphorylated S6 ribosomal protein (5364, Cell Signaling Technology, USA), rabbit anti-CDP (cux1) (sc-13024, Santa Cruz Biotechnology, USA), rabbit anti-Ctip2 (ab28448, Abcam, USA), rabbit anti-Tbr1 (ab31940, Abcam, USA), rabbit anti-ACIII (sc-588, Santa Cruz Biotechnology, USA), rabbit anti-p62 (PM045, MBL, USA), rabbit anti-Atg5 (NB110-53818, Novus Biologicals, USA), rabbit anti-Ki67 (ab15580, Abcam, USA), rabbit anti-PH3 (ab5176, Abcam, USA), rat anti-BrdU (ab6326, Abcam, USA), and rabbit anti-Arl13b

(17711-1-AP, Proteintech, USA). The next day, sections were washed two times with PBS for 10 minutes each. After washing, they were incubated 1 hour at room temperature with the following secondary antibodies: Alexa Fluor 555-conjugated goat antibody to mouse (A21422, Thermo Scientific, USA), Alexa Fluor 488-conjugated goat antibody to mouse (A11001, Thermo Scientific, USA), Alexa Fluor 555-conjugated goat antibody to rabbit (A21428, Thermo Scientific, USA), and Alexa Fluor 488-conjugated goat antibody to rabbit (A11008, Thermo Scientific, USA). After incubation, they were washed two times with PBS for 10 minutes each. The sections were mounted with prolong gold antifade reagent with DAPI (P36931, Thermo Scientific, USA). We acquired images using a Zeiss LSM780 confocal microscope. For bin analysis, total cortex was divided in ten equally spaced bins between ventricular surface and pial surface and the number of migrating neurons present in each bin was quantified. To analyze the disruption of cortical layer, fluorescence intensities for each cortical layer makers (Cux1, Ctip2, and Tbr1) from each bin were measured and normalized (La Fata et al., 2014). Manders co-localization analysis was performed using Fiji software (http://fiji.sc/Colocalization_Analysis). Neurolucida software (MBF Bioscience, USA) was used to create morphological reconstruction for neuronal polarity analysis. The researcher examining the histological sections was not blinded to the treatments.

QUANTIFICATION AND STATISTICAL ANALYSIS

All experiments requiring the use of animals, directly or as a source of cells, were subjected to randomization. We defined 'ciliated cells' as cells having a $\geq$ 1 μm long ciliary structure (Lee et al., 2012b). Sample sizes were predetermined based on the variability observed in preliminary and similar experiments. The researchers were not blinded to allocation during experiments or outcome analysis, except for the video-EEG monitoring. Statistical parameters including the defnition and exact values of n (number of cells and experiments), distribution and deviation are reported in figures and corresponding legends. Data are represented as means ± SEM and analyzed using Student's t test or ANOVA where appropriate, using GraphPad Prism 6 (GraphPad Software, La Jolla, CA). A Bonferroni post hoc test was used to analyze for significant differences in the ANOVA test. A P value less than 0.05 was considered statistically significant.